Enhanced eosinophilic inflammation associated with antibody and complement-mediated pneumonic insults in severe COVID-19

Dong-Min Kim
Chosun University College of Medicine
Jun-Won Seo
Chosun University College of Medicine
Yuri Kim
Seoul National University College of Medicine
Jooyeon Lee
Chungnam National University School of Medicine
Uni Park
Seoul National University College of Medicine
Na-Young Ha
Seoul National University College of Medicine
Jaemoon Koh
Seoul National University College of Medicine
Hyoree Park
Seoul National University College of Medicine
Jae-Won Lee
Seoul National University College of Medicine
Hyo-Jin Ro
Seoul National University College of Medicine
Na Ra Yun
Chosun University College of Medicine
Da Young Kim
Chosun University College of Medicine
Sung Ho Yoon
Chosun University College of Medicine
Yong Sub Na
Chosun University College of Medicine
Do Sik Moon
Chosun University College of Medicine
Sung-Chul Lim

Chosun University College of Medicine
Choon-Mee Kim
Chosun University College of Medicine
Kyeongseok Jeon
Seoul National University College of Medicine
Jun-Gu Kang
Jeonbuk National University
Hyeongseok Jeong
Chungnam National University School of Medicine
Jungok Kim
Chungnam National University School of Medicine
Shinhyea Cheon
Chungnam National University School of Medicine
Kyung Mok Sohn
Chungnam National University School of Medicine
Jae Young Moon
Chungnam National University School of Medicine
Sungmin Kym
Chungnam National University Sejong Hospital
Myung-Shin Lee
Eulji University School of Medicine
Hyun-Je Kim
Samsung Advanced Institute for Health Sciences & Technology
Woong-Yang Park
Samsung Advanced Institute for Health Sciences & Technology
Hyun-Woo Shin
Seoul National University College of Medicine
Hye-Young Kim
Seoul National University College of Medicine
Chung-Hyun Cho
Seoul National University College of Medicine
Yoon Kyung Jeon
Seoul National University College of Medicine
Yeon-Sook Kim
Chungnam National University School of Medicine
Nam-Hyuk Cho (chonh@snu.ac.kr)
Seoul National University College of Medicine

Research Article

Keywords: COVID-19, SARS-CoV-2, eosinophilic inflammation, pneumonia

Posted Date: November 3rd, 2020

DOI: https://doi.org/10.21203/rs.3.rs-101027/v1

Enhanced eosinophilic inflammation associated with antibody and complement-mediated pneumonic insults in severe COVID-19

Dong-Min Kim[1,13,*], Jun-Won Seo[1,13], Yuri Kim[2,3,4,13], Jooyeon Lee[5, 13], Uni Park[2,3,13], Na-Young Ha[2,3,4,13], Jaemoon Koh[6,13], Hyoree Park[2,3], Jae-Won Lee[2,3], Hyo-Jin Ro[2,3], Na Ra Yun[1], Da Young Kim[1], Sung Ho Yoon[1], Yong Sub Na[1], Do Sik Moon[1], Sung-Chul Lim[7], Choon-Mee Kim[8], Kyeongseok Jeon[2,3], Jun-Gu Kang[9], Hyeongseok Jeong[5], Jungok Kim[10], Shinhyea Cheon[5], Kyung Mok Sohn[5], Jae Youg Moon[10], Sungmin Kym[10], Myung-Shin Lee[11], Hyun-Je Kim[12], Woong-Yang Park[12], Hyun-Woo Shin[3], Hye-Young Kim[3], Chung-Hyun Cho[3], Yoon Kyung Jeon[6], Yeon-Sook Kim[5,*], and Nam-Hyuk Cho[2,3,4,*]

[1]Department of Internal Medicine, Chosun University College of Medicine, Gwangju, Republic of Korea.

[2]Department of Microbiology and Immunology, [3]Department of Biomedical Sciences, Seoul National University College of Medicine, Seoul, Republic of Korea.

[4]Institute of Endemic Disease, Seoul National University Medical Research Center and Bundang Hospital, Seoul, Republic of Korea.

[5]Department of Internal Medicine, Chungnam National University School of Medicine, Daejeon, Republic of Korea.

[6]Department of Pathology, Seoul National University College of Medicine, Seoul, Republic of Korea

[7]Department of Pathology, [8]Premedical Science, Chosun University College of Medicine,

Gwangju, Republic of Korea.

[9]Korea Zoonosis Research Institute, Jeonbuk National University, Iksan, Republic of Korea.

[10]Department of Internal Medicine, Chungnam National University Sejong Hospital, Sejong, Republic of Korea.

[11]Department of Microbiology and Immunology, Eulji University School of Medicine, Daejeon, Republic of Korea.

[12]Department of Health Sciences and Technology, Samsung Advanced Institute for Health Sciences & Technology, Sungkyunkwan University, Seoul, South Korea.

[13]These authors contributed equally.

*Correspondence: Dong-Min Kim (drongkim@chosun.ac.kr), Yeon-Sook Kim (alice@cnuh.co.kr), and Nam-Hyuk Cho (chonh@snu.ac.kr)

Abstract

Despite the worldwide effect of the Coronavirus disease 2019 (COVID-19) pandemic, the underlying mechanisms of fatal viral pneumonia remain elusive. Here, we conducted kinetic profiling of respiratory leukocytes and associated inflammatory mediators to show that severe COVID-19 is associated with delayed but enhanced eosinophilic inflammation when compared to mild cases. In addition, we confirmed increased Th2-biased adaptive immune responses, accompanying overt complement activation, in the severe group. Moreover, enhanced antibody responses and complement activation was associated with disease pathogenesis as evidenced by formation of immune complexes and membrane attack complexes in airways and vasculature of lung biopsies from a fatal case, as well as by enhanced hallmark gene set signatures of FcγR signaling and complement activation in myeloid cells of respiratory specimens from severe COVID-19 patients. We also observed expression of viral antigen in lung epithelial and endothelial cells without producing viruses during late stage of COVID-19, indicating abortive viral infection which may further fuel antibody responses and aggravate immune-complex-mediated inflammation. These results suggest that SARS-CoV-2 infection may drive scripted specific innate immune responses, including eosinophilic inflammation, and subsequent pulmonary pathogenesis via enhanced Th2-biased immune responses, which might be crucial drivers of severe pneumonia in COVID-19 patients.

Keywords: *COVID-19, SARS-CoV-2, eosinophilic inflammation, pneumonia*

Introduction

Severe acute respiratory syndrome coronavirus-2 (SARS-CoV-2)[1] has been rapidly spreading worldwide since Dec. 2019 with an average mortality rate of approximately 3.2% (https://covid19.who.int). The primary cause of disease fatality is severe pneumonia, resulting in acute respiratory syndrome (ARDS).[2] Around 80% of confirmed cases are asymptomatic or have mild symptoms, including fever, cough, sore throat, and myalgia, whereas the rest often develop severe pneumonia requiring supplemental oxygen therapy.[3,4] The most common finding of radiological imaging is bilateral, ground-glass opacity in the periphery of the lungs.[4] The mechanisms underlying this varying degree of pneumonia severity observed in COVID-19 patients remain elusive.[5] In particular, the dynamics of pathologic inflammation and the central culprits of pneumonic progression leading to severe ARDS and death still remain unclear, despite numerous studies profiling systemic immune signatures.[6,7]

In order to characterize the pathogenic hallmarks of severe pneumonia in COVID-19 patients, we performed kinetic analysis of inflammatory features of specimens collected from confirmed patients with various degrees of clinical symptoms. We systematically analyzed inflammatory components and leukocytes in bronchoalveolar lavage fluids (BALFs), sputa, lung tissue biopsies, and bloods to characterize kinetic responses of pulmonary inflammation upon viral infection. This extensive analysis revealed that severe COVID-19 is associated with enhanced eosinophilic pulmonary inflammation, as identified by cytological analysis and detection of granular contents derived from the inflammatory cells. In addition, kinetic profiling of inflammatory mediators, including various cytokines and chemokines, and titration of antibodies against a viral antigen revealed emerging Th2-biased adaptive immune responses, coupled to

overt complement activation, especially in the severe group. In addition, we observed extensive immune complexes and membrane attack complexes in pulmonary airways and vasculatures of lung biopsies from a fatal case. Moreover, persistent expression of viral antigens, potentially via abortive infection, in inflamed lungs at late stage may irreversibly aggravate antibody and complement-mediated pulmonary damage in fatal COVID-19. These results suggest that SARS-CoV-2 infection may drive scripted specific innate immune responses, including eosinophilic inflammation, and subsequent Th2-biased antigen-specific immune responses, which may contribute to COVID-19 associated severe pneumonia.

Results and Discussion

Baseline characteristics of the confirmed patients included in this study are summarized in Supplementary Table S1 and Fig. S1. The mild group includes 36 patients who were asymptomatic, with mild respiratory symptoms but no detectable pneumonia, or with mild to moderate pneumonia determined by chest imaging and clinical symptoms. The severe group includes 16 patients who suffered from severe pneumonia requiring high flow oxygen supply and/or mechanical ventilation. All the patients in the severe group survived and were discharged, except one patient (P15) who succumbed to death due to fatal ARDS. The patients were also divided into two sets: Group 1 includes 15 patients (10 mild and 5 severe group patients) who provided blood and respiratory specimens at different time points after symptoms onset. Group 2 includes 37 patients (26 mild and 11 severe patients) who provided respiratory specimens during the acute phase of COVID-19.

First, we investigated the potential association of viral loads of respiratory secretions with

systemic inflammation, as indicated by the levels of C-reactive proteins (CRP) in plasma.[8] The kinetics of viral loads in upper (nasopharyngeal and throat swabs) and lower (sputa and BALFs) respiratory tracts were not significantly different between severe and mild groups (Fig. 1a), as previously reported.[9,10] However, the levels of CRP in plasma were more significantly elevated in severe patients, especially during the first 20 days after symptom onset and peaking around day 10 (D10) (Fig. 1b). Therefore, viral loads measured in respiratory secretions may not be significantly associated with disease severity and systemic inflammation in COVID-19 patients.

To investigate the potential causative factors driving severe pulmonary inflammation during the acute phase of COVID-19, we tried to directly analyze the inflammatory cells and mediators in respiratory specimens. 45 BALFs and sputa samples collected from patient groups 1 and 2 at various time points after symptom onset were analyzed using H&E stained cytologic specimens to identify types and proportions of immune cell subsets infiltrating infected lungs (Fig. 2a and Supplementary Table S2). Despite wide variation among the specimens, BALFs and sputa from COVID-19 patients mainly contained PMNs (mostly neutrophils, mean ± S.D.: 46.8 ± 34.3% in total leukocytes), monocytes/macrophages (37.5 ± 32.7%), and a few lymphocytes (11.6 ± 12.2%). We also observed 48.9% (22/45) of the respiratory specimens included eosinophils (4.3 ± 7.3%) (Fig. 2a and Supplementary Table S2). When we compared the level of each inflammatory cell type between mild and severe patients, the relative proportion of all the cell types were not significantly different between the groups, although eosinophils were slightly higher in the mild group (6.0 ± 9.4%) than severe patients (2.8 ± 4.6%, $p = 0.18$) (Supplementary Table S2).

In order to characterize the immune cell population in detail and compare them with systemic leukocytes in COVID-19 patients, five paired BALFs and blood leukocytes collected from three

severe patients at the indicated day after symptom onset were directly applied for flow cytometric analysis. We identified the relative proportions of myeloid cells, including $CD14^+$ monocytes/macrophages and $SSC^{High}/CD14^-$ PMNs, among BALFs' and blood leukocytes, as well as $CD3^+$ T cells, $CD20^+$ B cells, $CD3^+/CD56^-$ natural killer (NK) cells, and $CD3^+/CD56^+$ NKT-like (denoted as NKT hereafter) cells,[11] based on expression levels of the indicated surface markers (Fig. 2b, Supplementary Fig. S2 – S5). In addition, PMNs were further defined by assessing the surface expression of CD16 and CD24.[12] T cells and NKT cells were also characterized by measuring CD4 and CD8 surface expression. As we observed in respiratory specimens by H&E staining, PMNs were the predominant inflammatory cells, ranging from 45.5% to 79.7% of lung-infiltrating leukocytes (Fig. 2b and Supplementary Fig. S3). This was followed by lymphoid cells, comprising 9.9% to 34.0%, and $CD14^+$ monocytes/macrophages, accounting for 2.8 ~ 11.1%. Among the PMNs in BALFs of severe patients, neutrophils were generally dominant in the inflamed lungs (36.3% ~ 62.1% among $CD45^+$ leukocytes) and 1.2 ~ 36.9% of leukocytes were eosinophils. It is notable that eosinophils were particularly elevated at 36.9% of total leukocytes in a BALF specimen from the fatal case P15 at D30. Among the lymphocyte population in BALFs from the severe cases, T cells were the dominant cell type, accounting for 72.3 ~ 89.6%, whereas B cells were barely detected (0.4 ~ 1.9%) (Fig. 2b, Supplementary Fig. S4). NK and NKT cells represented 2.3 ~ 9.6% and 3.7 ~ 11.5% of pulmonary lymphocytes, respectively. The ratio of $CD8^+$ and $CD4^+$ T cell in the respiratory specimens fluctuated (1.6 at D14, 0.6 at D20, 1.1 at D27, 1.0 at D30, and 1.9 at D39), but $CD8^+$ T cells generally predominated, suggesting a potential role of cytotoxic T cell responses in the respiratory tract of severe pneumonia (Fig 2b: right panel, and Supplementary Fig. S5). It is interesting to note that the majority of pulmonary NKT cells were CD8-positive (Supplementary

156 Fig. S5).

157 To assess the kinetic changes of immune cell types in respiratory specimens of COVID-19
158 patients, the relative proportion of each cell type was measured over time after symptom onset by
159 H&E staining and flow cytometry (Fig. 2c and d). Despite individual variations and fluctuations
160 among the specimens, PMNs, primarily neutrophils, were sustained in respiratory specimens
161 from severe cases, but rapidly declined in mild patients during the first 20 days after symptom
162 onset. Monocytes/macrophages also gradually decreased after an initial peak around D10 after
163 symptom onset in both mild and severe groups (Fig. 2c), whereas lymphocytes gradually
164 increased with more rapid response in mild patients than the severe group (Fig. 2d). Interestingly,
165 eosinophils were detectable in 55% (11/20) of specimens from mild patients during the first 10
166 days after symptom onset, whereas their infiltration was rather delayed and peaked during D10-
167 20 in severe cases (Fig. 2d). Eosinophil-positive rate in severe patients' sample was 64.0%
168 (16/25) when assessed by H&E and flow cytometry.

169 Since we observed pulmonary infiltration of PMNs, including neutrophils and eosinophils, we
170 measured the levels of inflammatory mediators derived from neutrophils (lipocalin-2, LCN;
171 calprotectin, CAPL)[13,14] and eosinophils (eosinophil-derived neurotoxin, EDN; eosinophilic
172 cationic protein, ECP)[15,16] in the respiratory specimens to assess innate cellular activation. LCN
173 and CALP were detected in specimens from both mild and severe patients (Fig. 3a). The relative
174 levels of both mediators were not significantly different between mild (mean ± S.D.: 977.8 ±
175 1366.4 ng/ml and 155.3 ± 478.7 mg/ml for LCN and CALP, respectively) and severe groups
176 (905.6 ± 1741.7 ng/ml and 44.7 ± 91.1 mg/ml for LCN and CALP, respectively), although
177 neutrophil responses were more sustained in severe cases (Fig. 3a). In contrast, levels of EDN
178 and ECP were generally higher in the respiratory specimens from severe patients (mean ± S.D.:

937.5 ± 1244.7 pg/ml and 60.5 ± 77.5 ng/ml for EDN and ECP, respectively) than mild cases (231.8 ± 375.6 pg/ml and 32.5 ± 62.3 ng/ml for EDN and ECP, respectively) (Fig. 3b). Of note, the levels of ECP were significantly higher in severe cases than the mild group (p = 0.0187). In addition, the level of mast cell tryptase (MCT) derived from mast cells upon activation was approximately 3.5 times higher in the severe group (31.1 ± 42.3 ng/ml) than mild cases (8.8 ± 4.4 ng/ml), although the difference was not statistically significant (p = 0.1141) (Fig. 3c). We also examined macrophage activation syndrome by measuring soluble CD163 (sCD163) molecules in the respiratory samples.[17,18] The levels of sCD163 peaked at around D10 in both mild and severe groups (Fig. 3d). The peak response was higher in severe cases than the mild group and the overall levels were significantly enhanced in severe patients, as previously suggested.[18] This confirms the role of macrophage infiltration and activation, potentially towards M2 phenotype, during the early phase of severe COVID-19 pneumoina.[19] Nevertheless, the concentration of sCD163 in severe cases after the initial peak response was similar to those of mild cases, suggesting a particularly intense contribution during the early phase of pneumonia progression. In addition, cytotoxic activity of CTLs and NK cells was not significantly different between mild and severe groups, when assessed by measuring granzyme A in respiratory specimens (Fig. 3e). Therefore, these results highlight the significant contribution of enhanced and sustained anaphylactic inflammation driven by infiltrating eosinophils in severe COVID-19 pneumonia,[20] together with an acute spike in macrophage activation during the early phase.[17]

To further define pulmonary inflammation associated with COVID-19 patients, we examined multiple cytokines, chemokines, and inflammatory mediators in 31 respiratory samples, including sputa and BALFs, collected from 11 patients (6 mild cases and 5 severe cases in group 1) at various time points after symptom onset (Fig. 4, Supplementary Table S3 and Fig. S6).

When we assessed the correlation of the overall levels of theses soluble proteins and grouped them by a hierarchical clustering based on the correlation coefficients of proteins, three distinct families of immune markers correlated positively with each other, although many of them showed broad positive correlation with outgroup members. Group I includes IL-4, IL-5, IL-13, TGF-β, CCL2 (MCP-1), CCL3 (MIP-1α), CCL5 (RANTES), CCL11 (Eotaxin-1), CXCL9 (MIG), C5a, and periostin; Group II contains IL-1α, IL-2, IL-7, IL-8, IL-15, TNF- α, CCL4 (MIP-1β), CX3CL1 (Fractalkine), and calprotectin; Group III includes IL-6, IL-10, IL-21, IFN-γ, CXCL10 (IP-10), CXCL16, and ECP. It is notable that Group I included type 2 cytokines (IL-4, IL-5, IL-13, and TGF-β) and chemoattractants (CCL3, CCL5, CCL11, periostin, and C5a) for granulocytes, including eosinophils.[16,21] On the other hand, Group II primarily include various cytokines linked to cytokine release syndrome (IL-1α, IL-6, IL-10, and TNF-α), while Group III includes type 1 cytokines and chemokines involved in cell-mediated immunity (IL-2, IL-7, IL-15, IFN-γ, CXCL10, and CXCL16), indicating functional correlation of soluble mediators in inflamed respiratory environment during the acute phase of COVID-19. When we compared the overall levels of cytokines and chemokines between mild and severe groups, only three inflammatory markers, IL-6 (mean ± S.D.: 2.8 ± 8.1 vs. 9.1 ± 14.1 ng/ml for mild and severe group, respectively), TGF-β (0.9 ± 1.9 vs. 3.2 ± 4.0 ng/ml for mild and severe group, respectively), and ECP (as noted above), were significantly higher in severe patients than the mild group (Supplementary Table S3). Systemic elevation of IL-6 is known to be a hallmark of respiratory failure and cytokine release syndrome in severe COVID-19,[22,23] and our data confirms a significant association of this inflammatory cytokine with disease severity even in the respiratory environment of COVID-19 patients. In addition, IL-6 also showed broad and

224 significant association with pro-inflammatory cytokines, as well as type 2 cytokines. ECP is
225 significantly correlated with proinflammatory cytokines, including IL-6 and TNF-α, in addition
226 to type 2 cytokines, such as IL-5 and IL-13 (Fig. 4a), suggesting a potential association of
227 eosinophilic inflammation with cytokine release syndrome and type 2 immune responses. TGF-
228 β was not significantly correlated with any other soluble markers, although it was grouped with
229 type 2 cytokines. Given the functional role of TGF-β in mucosal immunity and eosinophilic
230 pneumonia,[24,25] a significant elevation of TGF-β in respiratory specimens from severe COVID-
231 19 patients can be indicative of eosinophilic and type 2 mucosal immune responses.
232 Since eosinophilic inflammation is associated with Th2-polarized immune responses in various
233 pulmonary disorders,[16,26] we next assessed viral antigen-specific antibody responses, with a
234 focus on specific isotypes in respiratory secretions and plasma from the patients. We speculated
235 that specific immune responses against the SARS-CoV-2 antigen are orchestrated by a Th2-
236 biased immune environment, which can drive preferential isotype switching of specific
237 antibodies in B cells toward specific subclasses, such as IgE.[27] Antibody responses against
238 SARS-CoV-2 N protein generally rose during the first 10 days after symptom onset, peaking at
239 D10-D20, and then gradually declining in the respiratory specimens, regardless of disease
240 severity (Fig. 5a). The levels of specific isotype responses against the viral antigen were not
241 significantly different between mild and severe groups, except IgG which was significantly
242 higher in severe cases, especially during D10-D20. The positive rate of anti-N-specific IgE
243 response was 46.7% (7/15) in specimens from the severe group and 41.7% (5/12) in those from
244 mild patients, indicating a general prevalence of IgE responses in respiratory tracts regardless of
245 disease severity. Since there have been several reports on the involvement of elevated

246 complement activation in the plasma of severe COVID-19 patients,[28-30] we also assessed the
247 levels of complement protein in the respiratory specimens. We detected significantly higher
248 levels of C3a with a peak response at around D10 in severe patients (Fig. 5b), indicating
249 concomitant complement activation with antibody responses in the respiratory tracts during the
250 acute phase of COVID-19. In order to examine antibody-dependent activation of the complement
251 pathway,[30] we examined the correlation of C3a concentration with anti-N IgM and IgG antibody
252 responses, which are the major isotypes involved in the classical pathway of complement
253 activation.[31] The concentration of C3a was significantly correlated with both IgM and IgG levels
254 when measured in the same respiratory specimen (Fig. 5c), suggesting activation of the classical
255 pathway elevated complement activation in the respiratory tract in severe COVID-19.
256 Next, we examined the systemic levels of antigen-specific antibody responses in plasma (Fig. 6a
257 and Supplementary Fig. S7). Anti-N IgG antibodies, including IgG1 and IgG3 (IgG2 and IgG4
258 were barely detected), gradually increased in the plasma of all 15 patients (10 mild and 5 severe
259 patients) examined. Specific IgA responses were detected in plasma from all the severe patients
260 and positive in seven out of ten mild patients. In the case of IgE, four out of five (80%) severe
261 cases showed detectable levels, whereas it was detectable in only two patients among ten (20%)
262 mild patients within 40 days after symptom onset (Supplementary Fig. S7). Antibody responses
263 were generally more prompt and pronounced in severe cases than the mild group (Fig. 6a and
264 Supplementary Fig. S7). Moreover, levels of all the antibody isotypes were significantly higher
265 in the severe group than mild patients. Notably, there was a consistent surge in specific IgE
266 levels against viral N protein with a peak response during D10-20 in all severe pneumonic
267 patients, except one (P13), indicating a prevalence of antigen-specific IgE responses in severe
268 patients. We assessed complement activation in the same set of plasma samples by measuring the

concentrations of C3a and C5a. As observed in respiratory specimens (Fig. 5b), levels of C3a and C5a were generally higher in plasma from severe patients (7.9 ± 1.3 μg/ml and 50.5 ± 20.3 ng/ml for C3a and C5a, respectively) than in mild group (1.2 ± 2.0 μg/ml and 38.9 ± 30.1 ng/ml for C3a and C5a, respectively) (Fig. 6b). The difference in C5a levels between mild and severe groups was statistically significant, as previously reported.[28] In addition, we observed a significant positive correlation of C5a levels with plasma IgG1 and IgG3 levels (Fig. 6c). These results confirm that viral antigen-specific antibody responses in plasma from severe patients is significantly higher than those from the mild group, as previously reported.[32,33] This might be functionally linked to systemic and persistent activation of the complement cascade in severe pneumonic patients, potentially through the classical pathway. In addition, systemic but transient surge of antigen-specific IgE responses, driven by enhanced eosinophilic inflammation and TGF-β response in the respiratory tracts of severe patients, could be a hallmark of pathogenic progression and Th2-biased mucosal immunity in pneumonic lungs of severe COVID-19 patients. In order to confirm the pathogenic contribution of antibody responses and complement activation in severe COVID-19, we carefully assessed kinetic responses in the respiratory specimens and plasma from the fatal case, P15, and performed histological and immunofluorescence analysis using two lung biopsies obtained during late stage (D36 and D48) of COVID-19 before succumbing to death at D59 (Fig. 7). Viral loads in respiratory specimens gradually declined after symptom onset and were barely detected after D30 (Fig. 7a), as observed in other surviving cases (Fig. 1). Even though plasma CRP levels peaked at D13 and decreased thereafter, the levels of lactate dehydrogenase (LDH) remained above normal range throughout the disease course (Fig. 7b), suggesting persistent cellular damage. Histopathologic examination of lung biopsies

291 from the deceased patient showed subpleural fibrosis and diffuse fibrin deposit at D36 after
292 symptom onset (Fig. 7c and d). Lung parenchyma was almost completely destroyed, evidenced
293 by the presence of interstitial thickening with fibrosis, smooth muscle proliferation, and
294 granulation tissue formation. Alveolar spaces contained some macrophages and hemorrhage,
295 some neutrophilic infiltration, and vascular congestion was observed in subpleural granulation
296 tissue. At D48, hemorrhage and congestion were observed in destroyed lung parenchyma and
297 focal pulmonary microthrombi were identified (Fig. 7d). We also observed parenchymal
298 destruction by cystic change and bronchiolar metaplasia of alveoli. Infiltration of some
299 lymphoplasma cells in fibrotic interstitium was noted and variable sized alveolar macrophages
300 and seromucinous fluid were observed in alveolar spaces. Interestingly, antibody responses (IgM,
301 IgG, and IgA) against viral N antigen in respiratory specimens peaked during D10-20, gradually
302 declined until D30, and THEN elevated again thereafter (Fig. 7e). The kinetic responses of C5a
303 in the respiratory samples were also biphasic, with second minor surge at D30-40, suggesting
304 antibody-dependent complement activation in the respiratory tract. In addition, a transient surge
305 of IgE response was observed right before the second rise of antibody and complement responses
306 on D26. Moreover, N-specific antibody responses in plasma were also biphasic with an initial
307 peak during D20-40 and a second rise after D50. Plasma C5a levels also showed a second surge
308 after D50, indicating concomitant systemic responses of antibody and complement activation.
309 These results suggest that a second round of antigenic stimulation may drive specific antibody
310 responses and associated complement activation, especially in the respiratory tract. Since there
311 was few viral release in respiratory specimens after D30, we suspected that there might be active
312 production of viral antigens without secretion of virus particles, i.e. abortive viral infection, in
313 inflamed lungs of COVID-19. Indeed, immunostaining of viral N antigen of lung biopsies

collected at D36 and D48, active expression was especially pronounced in vascular walls, including endothelial cells, as well as in a few epithelial cells (Fig. 7f). Detection of viral antigen and/or viral RNA in endothelial cells and/or epithelial cells of tissue biopsies from COVID-19 patients has also been confirmed in other reports.[19,34-39] In addition, formalin-fixed paraffin-embedded lung tissue subjected to immunohistochemical staining with anti-C5b-9 antibody showed massive deposition of membrane attack complexes (MACs) in vascular walls, especially subendothelial and smooth muscle layers, bronchial epithelial cells, as well as inflammatory cells including macrophages and lymphocytes (Fig. 8a). The intensity of C5b-9 staining in pulmonary vessels was increased at D48 when compared to that of D38. The gradual increase of creatine phosphokinase (CPK) in the patient's plasma after D40 may also reflect progressive cellular damage of vascular smooth muscle layer upon MAC formation and/or myocardial injury in fatal COVID-19 patients (Fig. 7b), as previously reported.[40,41] Moreover, deposition of IgG immune complexes in hyaline membranes and fibrin deposits within luminal spaces of airways and vascular capillaries emerged at D36 and increased at D48 (Fig. 8b and Supplementary Fig. S9). These results strongly suggest that active expression of viral antigen without producing viral particles during late stage of severe COVID-19 drives a second cycle of antibody responses accompanying complement activation. Concomitant immune complex formation and complement activation may drive irreversible pulmonary damage in fatal COVID-19.[42] Evidence of fatal COVID-19 vasculopathy accompanying deposition of immune complexes and/or complement components inside vascular walls in multiple organs have also been reported in recent studies.[43,44]

Based on our observations of extensive kinetic analyses using respiratory specimens, we propose that sustained eosinophilic inflammation is followed by Th2-biased adaptive immune responses,

as evidenced by enhanced viral antigen-specific antibody responses and concomitant complement activation, in severe COVID-19. Overt antibody responses together with complement activation potentially contribute to the progression and pathogenesis of severe COVID-19. Nevertheless, significant infiltration of eosinophils into lungs of COVID-19 patients during the acute phase of infection can be either protective or detrimental.[45] Although peripheral blood eosinopenia at initial presentation might be associated with severe COVID-19, as we and others observed in COVID-19 patients (see complete blood count results in Supplementary Fig. S8),[46] sustained and enhanced eosinophilic inflammation in respiratory tracts of COVID-19 is consistently observed in severe cases (Fig. 2 and 3b). Interestingly, rapid eosinophilic infiltration into infected lungs was often observed in mild patients within 10 days after symptom onset, whereas eosinophil infiltration is delayed but prolonged and eosinophilic inflammation is significantly increased, as indicated by enhanced responses of ECP and EDN, in respiratory tracts of severe pneumonic cases. Eosinophil response during the early stage of viral infection can orchestrate antiviral responses to respiratory viruses by producing reactive oxygen species and eosinophil-derived RNases (EDN/RNase2 and ECP/RNase3).[45] However, sustained eosinophilic inflammation may represent an acute type I hypersensitivity reaction, which is often functionally linked to Th2-polarizing respiratory environment.[26] Enhanced TGF-β responses, mast cell activation, and more prompt and robust viral antigen-specific antibody responses, including IgE isotypes, strongly support the potential pathogenic role of eosinophilic inflammation and Th2-biased mucosal immunity in severe COVID-19.[6] Moreover, acute and transient surge of eosinophilia in inflamed lungs, as observed in the fatal case (P15), might be a critical driver of irreversible lung damage associated with lethal outcome in severe COVID-19 patients. Recently, the association of systemic eosinophilic inflammation with various COVID-

19-associated syndromes has been reported by several studies.[47,48] Interestingly, we observed transient elevation, peaking at D10, of macrophage activation as assessed by sCD163 levels in respiratory samples of severe patients (Fig. 3d). The role of alternatively activated (M2 type) macrophages in eosinophilic pulmonary inflammation has also been previously documented.[16,49] Therefore, macrophage activation syndrome often observed in severe COVID-19 patients[17] can be functionally linked to eosinophilic pulmonary inflammation. While the causal relationship and precise mechanisms mediating innate cellular interactions during pathologic progression remain to be elucidated, our kinetic analyses reveal concomitant elevation of pulmonary inflammation, potentially driven by macrophage, eosinophil, and mast cell activation in severe COVID-19 (Fig. 3). Given that early viral loads in respiratory tracts of COVID-19 patients does not seem to enhance pulmonary inflammation by innate cellular activation, host factor(s) specifically driving inflammation need to be determined in future studies.

Our second critical finding is the potential role of enhanced antibody responses accompanying elevated complement activation in disease pathogenesis of severe COVID-19. As mentioned above, kinetic analyses of respiratory specimens revealed sustained and higher eosinophilic inflammation as a potential driver for Th2 immune responses in severe COVID-19. A recent immune profiling study using peripheral blood mononuclear cells and plasma samples from 113 patients with moderate or severe COVID-19 also showed an association of an increase in multiple type 2 effectors, including IL-5, IL-13, IgE, and eosinophils, with disease severity.[6] More rapid and robust antibody responses specific to SARS-CoV-2 antigens, including spike and nucleocapsid (N), have been consistently observed in many other studies.[32,33,50] Here, we confirmed enhanced antibody responses against viral N antigen in plasma, as well as respiratory IgG response, in severe patients. In addition, kinetic analysis revealed earlyer peak response

(D10-20) of systemic IgA and IgE, as well as respiratory antibodies, followed by systemic IgG responses which peak at D20-30 in severe cases; meanwhile, all these isotypes peaked at D20-30 in plasma from mild group patients (Fig. 5). Earlier predominance of IgA and IgE responses might be due to pulmonary eosinophilic inflammation and enhanced TGF-β responses in respiratory mucosal environment of severe patients.[16,24,26] Moreover, complement activation was generally higher in the respiratory tracts and systemic circulation of severe patients than mild group, and correlated well with the levels of IgM and IgG responses in the respiratory environment, suggesting increased activation of antibody-dependent classical pathway. While the contribution of both alternative and lectin-dependent pathways during SARS-CoV-2 infection can not be excluded,[44] complement C1q levels in plasma from severe cases were lower than mild cases,[30] indicating systemic C1q depletion due to antibody-dependent classical pathway of complement activation in severe cases. Nevertheless, it remains unknown whether enhanced antibody responses and accompanying complement activation are directly and functionally associated with pathogenic progression of severe COVID-19.[51,52] Enhanced antibody responses are not necessarily critical for antiviral immunity, since viral copy numbers in respiratory secretions declined to baseline during peak antibody responses (D20-30) and there was no significant difference in viral loads between mild and severe patients (Fig. 1a). In addition, systemic viremia has been rarely detected in the majority of COVID-19 patients regardless of disease severity.[53,54] Rather, we suspected that Fcγ receptor (FcγR)-mediated inflammation upon crosslinking by immune complexes induces lung tissue damage through activation of the complement pathway and MAC formation (Fig 8).[52] Since viral release from infected host cells rapidly decreased, rising antibodies might bind to cells expressing the viral antigens. Infected

405 epithelial and endothelial cells (Fig. 7f) in lungs of COVID-19 patients could be primary targets
406 for the antigen-antibody immune complexes. Gradually increased IgG deposition on the luminal
407 surfaces of airways and vasculatures observed in lung biopsies from a fatal case (Fig. 8b)
408 strongly supports the pathogenic role of the immune complex-mediated pathway. We also often
409 observed large immune complexes including detached epithelial layers or N antigen-positive
410 cells in airway lumens (Fig 8b and Supplementary Fig. S9). Expression of viral antigens in
411 epithelial and endothelial cells without producing viral particles, indicating abortive viral
412 infection, during late stage COVID-19 may further fuel antibody responses and aggravate
413 immune-complex-mediated inflammation, including complement activation (Fig 7d and Fig. 8),
414 as well as activating effector leukocytes by engaging various members of FcγR.[52] To confirm this,
415 we retrieved gene expression data sets from recent single cell RNA sequencing (scRNA seq)
416 studies[55,56] and analyzed the hallmark gene set scores for each signaling pathway.[57] In the initial
417 analyses of signature gene set scores for inflammation in major leukocyte populations (Fig. 9a),
418 myeloid cells including monocytes, macrophages, and dendritic cells, as well as neutrophils
419 showed prominent increase in hallmark inflammation scores when compared to those of healthy
420 control group (Fig. 9b). Analysis of scRNA seq data sets from mononuclear phagocytes
421 (monocytes, macrophages, and dendritic cells) and neutrophils showed significantly higher levels
422 of hallmark gene set scores for both FcγR signaling and complement activation in severe group
423 than those of mild cases (Fig. 9c). These results clearly indicate a significant role of FcγR
424 signaling and complement activation in inflammatory responses and pathogenic contributions by
425 phagocytic cells.[17,29,52]
426 In conclusion, our current kinetic analyses of respiratory specimens from COVID-19 patients
427 clearly reveal an association of eosinophilic pulmonary inflammation with severe pneumonic

pathogenesis. These observations require further confirmation with extensive research of the pathogenesis of eosinophilic inflammation and its association with pathogenic role of antibody responses and complement activation in order to establish proper therapeutic strategies against severe pneumonia often resulting in fatal outcome in COVID-19. Moreover, potential abortive viral infections during late stage of COVID-19 may need to be carefully controlled to abrogate the pathologic contribution by immune-complex and complement-mediated inflammation.

Methods

Ethnical statement

The current research was approved by the institutional review boards of Chosun University Hospital (IRB no.: 2020-02-011), Chungnam National University Hospital (IRB no.: CNUH2017–12–004), and Seoul National University Hospital (IRB no.: C-1509-103-705). This study was performed in accordance with the ethical standards laid down in the 1964 declaration of Helsinki and all subsequent revisions. This study was conducted with informed consent from patients or their legal guardians.

Patient groups

General information on the clinical courses and baseline characteristics of the COVID-19 patients included in this study are summarized in Supplementary Table S1 and Fig. S1. The patients were divided into two groups based on disease severity. The mild group includes 36 patients who were asymptomatic, with mild respiratory symptoms but no detectable pneumonia, or with mild to moderate pneumonia determined by chest imaging and clinical symptoms. The severe group includes 16 patients who suffered from severe pneumonia requiring high flow

oxygen supply and/or mechanical ventilation. Among the severe group patients, all the patients survived and were discharged, except one patient (P15) who succumbed to death due to fatal ARDS. The patients were also divided into two sets. Group 1 includes 15 patients (10 mild and 5 severe group patients) who provided blood and respiratory specimens at different time points after symptoms onset. Group 2 includes 37 patients (26 mild and 11 severe patients) and provided respiratory specimens during the acute phase of COVID-19. Some of the clinical data from three patients (ID: 1, 11, and 12) were included in our previous preprint paper (DOI:10.21203/ rs.3.rs-23607/v1).

Cytological analysis

BALFs and sputa samples collected from the patients were smeared on glass slides immediately after collection. The slides were then immediately fixed with 95% ethanol in a Coplin jar. After fixing the slides, hematoxylin and eosin (H&E) staining was performed. The presence and relative proportions of various leukocyte subsets were estimated under light microscope independently by two experienced pathologists and consensus was reached under multi-head microscope.

Flow cytometry

Peripheral blood leukocytes and mononuclear cells (PBMCs) were prepared by standard density gradient centrifugation with Histopaque-1077 and 1119 (Sigma-Aldrich, St. Louis, MO, USA) in a biosafety level 3 laboratory in Seoul National University. Isolated blood leukocytes were directly stained with antibodies listed below for flow cytometry in a biosafety level 3 laboratory. Cells in BALFs and lung biopsies were directly prepared and analyzed on the collection day in a biosafety level 3 laboratory, as previously described.[58] Dead cells were stained with Zombie Aqua Fixable Viability Dye (BioLegend, San Diego, CA, USA). Cells were stained with the

following sets of antibodies differentially labeled with the indicated fluorochrome; anti-CD4-Alexa488, anti-CD8-PerCP or APC, anti-CD14-BV605, anti-CD16-Alexa700, anti-CD24-BV421, anti-CD45-PerCP-Cy5.5, anti-CD206-Alexa488, anti-HLA-DR-BV711 (from BioLgend), anti-CD3-PE-CF594 or Pacific blue, anti-CD20-APC/H7, and anti-CD56-APC (from BD Bioscience). Cell were then fixed with a fixation buffer (BD Bioscience) and analyzed using a FACS Fortessa II flow cytometer (BD Biosciences). Data were analyzed using Flowjo software (Tree Star, Ashland, OR, USA). Gating strategies for flow cytometric analyses are summarized in Supplementary Fig. S2.

Quantitation of cytokines and chemokines

Cytokine/chemokine levels in human respiratory samples (BALFs and sputa) were measured by a luminex multiplex assay system (Luminex, Austin, TX, USA) after gamma-irradiation (30 kGy). Luminx assay was run according to the manufacturer's instructions, using a customized human cytokine multiplex panel (R&D Systems, Inc. Minneapolls, MN, USA). The panel included: CCL2/JE/MCP-1, CCL3/MIP-1α, CCL4/MIP-1β, CCL5/RNATES, CCL11/Eotaxin, complement component C5a, CX3CL1/Fractalkine, CXCL9/MIG, CXCL10/IP-10/CRG-2, CXCL16, IFN-γ, IL-1α/IL-1F1, IL-2, IL-4, IL-5, IL-6, IL-7, IL-8/CXCL8, IL-10, IL-12/IL-23p40, IL-13, IL-15, IL-21, Periosin/OSF-2, TNF-α, TGF-β, sCD163, and granzyme A. Assay plates were measured using a Luminex 100/200TM analyzer (Luminex, Austin, TX, USA). Standard curve for each cytokine/chemokine was drawn using the supplied cytokine/chemokine standard and determined with the best fit algorithm using MasterPlex QT 2010 software (MiraiBio, Hitachi, CA, USA). IL-33 (Invitrogen, Carlsbad, CA, USA), lipocalin-2 (Abcam, Cambridge, UK), EDN, and MCT (Cusabio, Houston, TX, USA) were quantified using human

ELISA kits according to the manufacturer's instruction. Concentration of ECP and calprotectin in respiratory specimens were measured via clinical diagnosis service from Seoul Clinical Laboratory (Seoul, Republic of Korea).

Enzyme-linked immunosorbent assay (ELISA)

To assess for SARS-CoV-2 N protein-specific antibody responses, 96-well immunoassay plates (Nunc, Waltham, MA, USA) were coated with 100 μL of purified antigen at a concentration of 1 μg/mL at 4 °C overnight. The plates were then blocked for 2 h at room temperature (RT) with PBS containing 5% skim milk. One hundred microliters of serially diluted plasma or respiratory samples were incubated for 2 h at RT. After washing with PBS containing 0.05% Tween20 (0.05% PBST), horseradish peroxidase (HRP)-conjugated mouse anti-human IgG1, IgG2, IgG3, IgG4, IgG, IgM, IgA or IgE antibody (Southern Biotech, Birmingham, AL, USA) was added and incubated for 1 h at RT. Wells were washed with 0.05% PBST and incubated with a 3,3′,5,5′-tetramethylbenzidine (TMB) peroxidase substrate solution (KPL, Gaithersburg, MD, USA) for 10min. The reactions were stopped by addition of a 1M phosphoric acid solution. Absorbance was measured at 450 nm using a microplate reader (Beckman Coulter, Brea, CA, USA). The cut-off titer for the ELISA was defined as the lowest titer showing an optical density (OD) over the mean OD plus 3× standard deviation (s.d.) from three control plasma samples (diluted 1:10) collected from healthy volunteers or three pneumonia patients who were never diagnosed with COVID-19.

Quantitation of viral loads

Real-time reverse transcription-polymerase chain reaction (RT-PCR) assay for detection of SARS-CoV-2 was performed according to the manufacturer's instructions (Kogenebiotech, Seoul, South Korea). Total RNAs were obtained from nasopharyngeal and throat swab samples (upper

518 respiratory tract) and sputa (lower respiratory tract). Primer sets targeting E and RdRP genes of
519 SARS-CoV-2 were used with a cut-off cycle threshold (Ct) value of higher than 38 cycles.

520 **Quantitation of complements**

521 Human complement assays were conducted using quantitative C3a and C5a ELISA kits
522 according to the manufacturer's instructions (Thermo Fisher Scientific, Waltham, MA, USA). In
523 brief, patients' plasma were incubated in microwells adsorbed with anti-human C3a or C5a
524 coating antibody for 2 h at RT, washed 6 times, and incubated with a biotin-conjugated anti-
525 human C3a or C5a antibody for 1 h. The plates were then washed 6 times followed by incubation
526 with streptavidin-HRP for 1 h. After washing the wells, TMB substrate solution was added and
527 further incubated at RT. The reaction was terminated by adding 1 M phosphoric acid and
528 absorbance was measured with a TECAN microplate reader (TECAN, Mannedorf, Switzerland)
529 at 450 nm.

530 **Immunohistochemistry and immunofluorescence assay using lung biopsies**

531 Histopathological analysis of lung biopsies was performed after fixation in 10% formalin and
532 embossing in paraffin. Tissue sections (4 μm thickness) were stained with hematoxylin and eosin
533 (H&E) and two experienced pathologists specialized in lung pathology evaluated the H&E slides
534 under a light microscope (Olympus BX-53; Olympus, Tokyo, Japan). For immunohistochemistry
535 and immunofluorescence analysis, paraffin-embedded tissue sections were placed at 55°C
536 overnight. Tissue sections were rehydrated by submerging in xylen sequentially for 15 min, 5
537 min, and 5 min, followed by immersion in 100%, 100%, 95%, 90%, 80%, and 70% ethanol in
538 serial order, for 3 min per step. For antigen retrieval, the slides were soaked and heated in HIER
539 buffer (10 mM Tri-sodium citrate, 0.05% Tween-20, pH 6) in the microoven for 20 min. After
540 blocking with a buffer containing 5% BSA and Fc blocker (BD Biosciences) for 1 h at room

temperature, autofluorescence emitted by lung tissues was inhibited by incubation with 0.1% Sudan Black solution for 20 min, followed by incubation with indicated antibody for 15 minutes. The antibodies used to detect specific antigens for immunostaining processes were rabbit polyclonal anti-SARA-CoV-2 N antibody was obtained from Sino biological (Beijing, China) and anti-CD31 and pan-cytokeratin (CK) antibodies purchased from DAKO (Carpinteria, CA, USA). Antibody binding to the cells in sections was detected using horseradish peroxidase (HRP) reaction kits (DAKO) for immunohistochemistry or Alexa488-, Alexa594-, Alexa-633 conjugated secondary antibodies (Molecular Probes) for immunofluorescence. Nuclear DNA was counterstained with 4,6-diamidino-2-phenylindole (DAPI). Confocal microscopy was performed using an OlympusFV3000 laser-scanning microscope (Olympus). All images were analyzed and processed using the Olympus Fluoview or Adobe Photoshop software.

Analysis of single cell RNA seq datasets of BALFs from COVID-19 patients.

We collected BALF single cell RNA seq (scRNA-seq) datasets from the Gene Expression Omnibus (GEO) under accession code GSE145926 and from FigShare (https://doi.org/10.6084/m9.figshare.12436517).[55,56] We applied quality control criteria to each data set (mitochondrial gene percentage < 0.15). After filtering, a total single cell of 182,140 were used for analysis. To remove batch effects across the two datasets, we used multi canonical correlation analysis 3 (CCA3) in Seurat3 R package.[59] Variably expressed genes were selected using the FindVariableGenes function in default parameters of Seurat v3.1.5.[59] Cell clustering and Uniform Manifold Approximation and Projection (UMAP) visualization were performed using the FindClusters and RunUMAP functions, respectively. The annotations of cell identity for each cluster were defined by the expression of known marker genes: epithelial cells, EFHC1 and MLF1; T/NK cells, IL32, KLRB1, and STMN1; B cell, CD19 and MS4A1; neutrophils,

LYN, FCGR3B, and ITGAX; monocyte/macrophage/dendritic cells, CD14, CCL2, CD68, FABP5, CD74, CLEC4C, KIT, CPA3, HPGD, and LTC4S. To score the hallmark gene sets for inflammation,[60] complement activation[60], and reactome FcγR activation,[61] data sets were downloaded from MsigDB (https://www.gsea-msigdb.org/gsea/msigdb) using the AddModuleScore function provided by the Seurat package and analyzed.

Statistical analysis

Data was analyzed using the Graph Pad Prism 5.01 software (GraphPad Software, La Jolla, CA, USA) and Microsoft Excel (Microsoft Office Professional Plus 2016). Statistical analyses were performed using a two-tailed Mann–Whitney U test, unpaired Student's *t*-test, or one-way analysis of variance (ANOVA) followed by Newman-Keuls t-test for comparisons of values among different groups. Spearman's rank test was used to analyze the correlation between variables. A p-value of < 0.05 was considered statistically significant.

Acknowledgement

This research was supported by a grant from the National Research Foundation of Korea (grant no. 2017M3A9E4061998), and a grant (2017N-ER5307/4834-300-210-13) from Korea Center for Disease Control and Prevention, funded by the government of South Korea. Y.K., U.P., N.Y.H., H.P., K.J., and J.G.K. received a scholarship from the BK21-plus education program provided by the National Research Foundation of Korea.

Potential conflicts of interest. All authors: No reported conflicts of interest.

References

1 Grp, C. S. The species Severe acute respiratory syndrome-related coronavirus: classifying 2019-nCoV and naming it SARS-CoV-2. *Nature Microbiology* **5**, 536-544, doi:10.1038/s41564-020-0695-z (2020).

2 Yang, X. *et al.* Clinical course and outcomes of critically ill patients with SARS-CoV-2 pneumonia in Wuhan, China: a single-centered, retrospective, observational study. *Lancet Respir Med*, doi:10.1016/S2213-2600(20)30079-5 (2020).

3 Kim, E. S. *et al.* Clinical Course and Outcomes of Patients with Severe Acute Respiratory Syndrome Coronavirus 2 Infection: a Preliminary Report of the First 28 Patients from the Korean Cohort Study on COVID-19. *J Korean Med Sci* **35**, e142, doi:10.3346/jkms.2020.35.e142 (2020).

4 Zhou, F. *et al.* Clinical course and risk factors for mortality of adult inpatients with COVID-19 in Wuhan, China: a retrospective cohort study. *Lancet* **395**, 1054-1062, doi:10.1016/S0140-6736(20)30566-3 (2020).

5 Tay, M. Z., Poh, C. M., Renia, L., MacAry, P. A. & Ng, L. F. P. The trinity of COVID-19: immunity, inflammation and intervention. *Nat Rev Immunol*, doi:10.1038/s41577-020-0311-8 (2020).

6 Lucas, C. *et al.* Longitudinal analyses reveal immunological misfiring in severe COVID-19. *Nature* **584**, 463-469, doi:10.1038/s41586-020-2588-y (2020).

7 Mathew, D. *et al.* Deep immune profiling of COVID-19 patients reveals distinct immunotypes with therapeutic implications. *Science* **369**, doi:10.1126/science.abc8511 (2020).

8 Li, H. *et al.* SAA is a biomarker to distinguish the severity and prognosis of Coronavirus Disease 2019 (COVID-19). *J Infect*, doi:10.1016/j.jinf.2020.03.035 (2020).

9 Pan, Y., Zhang, D., Yang, P., Poon, L. L. M. & Wang, Q. Viral load of SARS-CoV-2 in clinical samples. *Lancet Infect Dis* **20**, 411-412, doi:10.1016/S1473-3099(20)30113-4 (2020).

10 He, X. *et al.* Temporal dynamics in viral shedding and transmissibility of COVID-19. *Nature medicine* **26**, 672-675, doi:10.1038/s41591-020-0869-5 (2020).

11 Peng, L. S. *et al.* Altered phenotypic and functional characteristics of CD3+CD56+ NKT-like cells in human gastric cancer. *Oncotarget* **7**, 55222-55230, doi:10.18632/oncotarget.10484 (2016).

12 Yu, Y. R. *et al.* Flow Cytometric Analysis of Myeloid Cells in Human Blood, Bronchoalveolar Lavage, and Lung Tissues. *Am J Respir Cell Mol Biol* **54**, 13-24, doi:10.1165/rcmb.2015-0146OC (2016).

13 Hara, A. *et al.* S100A9 in BALF is a candidate biomarker of idiopathic pulmonary fibrosis. *Resp Med* **106**, 571-580, doi:10.1016/j.rmed.2011.12.010 (2012).

14 Pechous, R. D. With Friends Like These: The Complex Role of Neutrophils in the Progression of Severe Pneumonia. *Front Cell Infect Mi* **7**, doi:ARTN 160 10.3389/fcimb.2017.00160 (2017).

15 Spencer, L. A., Bonjour, K., Melo, R. C. & Weller, P. F. Eosinophil secretion of granule-derived cytokines. *Frontiers in immunology* **5**, 496, doi:10.3389/fimmu.2014.00496 (2014).

16 Rosenberg, H. F., Dyer, K. D. & Foster, P. S. Eosinophils: changing perspectives in health

and disease. *Nat Rev Immunol* **13**, 9-22, doi:10.1038/nri3341 (2013).

17 Merad, M. & Martin, J. C. Pathological inflammation in patients with COVID-19: a key role for monocytes and macrophages. *Nat Rev Immunol* **20**, 355-362, doi:10.1038/s41577-020-0331-4 (2020).

18 Shoenfeld, Y. Corona (COVID-19) time musings: Our involvement in COVID-19 pathogenesis, diagnosis, treatment and vaccine planning. *Autoimmunity Reviews* **19**, doi:ARTN 102538 10.1016/j.autrev.2020.102538 (2020).

19 Zeng, Z. *et al.* Pulmonary Pathology of Early Phase COVID-19 Pneumonia in a Patient with a Benign Lung Lesion. *Histopathology*, doi:10.1111/his.14138 (2020).

20 Reber, L. L., Hernandez, J. D. & Galli, S. J. The pathophysiology of anaphylaxis. *J Allergy Clin Immunol* **140**, 335-348, doi:10.1016/j.jaci.2017.06.003 (2017).

21 Blanchard, C. *et al.* Periostin facilitates eosinophil tissue infiltration in allergic lung and esophageal responses. *Mucosal Immunol* **1**, 289-296, doi:10.1038/mi.2008.15 (2008).

22 Mazzoni, A. *et al.* Impaired immune cell cytotoxicity in severe COVID-19 is IL-6 dependent. *J Clin Invest*, doi:10.1172/JCI138554 (2020).

23 Gubernatorova, E. O., Gorshkova, E. A., Polinova, A. I. & Drutskaya, M. S. IL-6: Relevance for immunopathology of SARS-CoV-2. *Cytokine Growth Factor Rev* **53**, 13-24, doi:10.1016/j.cytogfr.2020.05.009 (2020).

24 Borsutzky, S., Cazac, B. B., Roes, J. & Guzman, C. A. TGF-beta receptor signaling is critical for mucosal IgA responses. *Journal of Immunology* **173**, 3305-3309, doi:DOI 10.4049/jimmunol.173.5.3305 (2004).

25 Katoh, S. *et al.* Elevated levels of periostin and TGF-beta1 in the bronchoalveolar lavage

fluid of patients with idiopathic eosinophilic pneumonia. *Asian Pac J Allergy Immunol*, doi:10.12932/AP-111018-0414 (2019).

26 De Giacomi, F., Vassallo, R., Yi, E. S. & Ryu, J. H. Acute Eosinophilic Pneumonia. Causes, Diagnosis, and Management. *Am J Respir Crit Care Med* **197**, 728-736, doi:10.1164/rccm.201710-1967CI (2018).

27 Scott-Taylor, T. H., Axinia, S. C., Amin, S. & Pettengell, R. Immunoglobulin G; structure and functional implications of different subclass modifications in initiation and resolution of allergy. *Immun Inflamm Dis* **6**, 13-33, doi:10.1002/iid3.192 (2018).

28 Carvelli, J. *et al.* Association of COVID-19 inflammation with activation of the C5a-C5aR1 axis. *Nature*, doi:10.1038/s41586-020-2600-6 (2020).

29 Cugno, M. *et al.* Complement activation in patients with COVID-19: A novel therapeutic target. *J Allergy Clin Immunol* **146**, 215-217, doi:10.1016/j.jaci.2020.05.006 (2020).

30 Wu, Y. *et al.* Clinical Characteristics and Immune Injury Mechanisms in 71 Patients with COVID-19. *mSphere* **5**, doi:10.1128/mSphere.00362-20 (2020).

31 Ricklin, D., Reis, E. S. & Lambris, J. D. Complement in disease: a defence system turning offensive. *Nat Rev Nephrol* **12**, 383-401, doi:10.1038/nrneph.2016.70 (2016).

32 Long, Q. X. *et al.* Antibody responses to SARS-CoV-2 in patients with COVID-19. *Nature medicine* **26**, 845-848, doi:10.1038/s41591-020-0897-1 (2020).

33 Wang, Y. *et al.* Kinetics of viral load and antibody response in relation to COVID-19 severity. *J Clin Invest*, doi:10.1172/JCI138759 (2020).

34 Colmenero, I. *et al.* SARS-CoV-2 endothelial infection causes COVID-19 chilblains: histopathological, immunohistochemical and ultrastructural study of seven paediatric cases. *Br J Dermatol*, doi:10.1111/bjd.19327 (2020).

675 35 Varga, Z. *et al.* Endothelial cell infection and endotheliitis in COVID-19. *Lancet* **395**,
676 1417-1418, doi:10.1016/S0140-6736(20)30937-5 (2020).
677 36 Hanley, B. *et al.* Histopathological findings and viral tropism in UK patients with severe
678 fatal COVID-19: a post-mortem study. *Lancet Microbe*, doi:10.1016/S2666-
679 5247(20)30115-4 (2020).
680 37 Borczuk, A. C. *et al.* COVID-19 pulmonary pathology: a multi-institutional autopsy
681 cohort from Italy and New York City. *Mod Pathol*, doi:10.1038/s41379-020-00661-1
682 (2020).
683 38 Yao, X. H. *et al.* Pathological evidence for residual SARS-CoV-2 in pulmonary tissues of
684 a ready-for-discharge patient. *Cell Res* **30**, 541-543, doi:10.1038/s41422-020-0318-5
685 (2020).
686 39 Ackermann, M. *et al.* Pulmonary Vascular Endothelialitis, Thrombosis, and Angiogenesis
687 in Covid-19. *N Engl J Med* **383**, 120-128, doi:10.1056/NEJMoa2015432 (2020).
688 40 Clark, J. F. The creatine kinase system in smooth muscle. *Mol Cell Biochem* **133-134**,
689 221-232, doi:10.1007/BF01267956 (1994).
690 41 Shi, L., Wang, Y., Wang, Y., Duan, G. & Yang, H. Meta-Analysis of Relation of Creatine
691 kinase-MB to Risk of Mortality in Coronavirus Disease 2019 Patients. *Am J Cardiol* **130**,
692 163-165, doi:10.1016/j.amjcard.2020.06.004 (2020).
693 42 Ward, P. A., Fattahi, F. & Bosmann, M. New Insights into Molecular Mechanisms of
694 Immune Complex-Induced Injury in Lung. *Frontiers in immunology* **7**, doi:ARTN 86
695 10.3389/fimmu.2016.00086 (2016).
696 43 Roncati, L. *et al.* Type 3 hypersensitivity in COVID-19 vasculitis. *Clin Immunol* **217**,

108487, doi:10.1016/j.clim.2020.108487 (2020).

44 Magro, C. *et al.* Complement associated microvascular injury and thrombosis in the pathogenesis of severe COVID-19 infection: A report of five cases. *Transl Res* **220**, 1-13, doi:10.1016/j.trsl.2020.04.007 (2020).

45 Lindsley, A. W., Schwartz, J. T. & Rothenberg, M. E. Eosinophil responses during COVID-19 infections and coronavirus vaccination. *J Allergy Clin Immunol* **146**, 1-7, doi:10.1016/j.jaci.2020.04.021 (2020).

46 Qin, C. *et al.* Dysregulation of immune response in patients with COVID-19 in Wuhan, China. *Clin Infect Dis*, doi:10.1093/cid/ciaa248 (2020).

47 Leis-Dosil, V. M., Saenz Vicente, A. & Lorido-Cortes, M. M. Eosinophilic Panniculitis Associated With COVID-19. *Actas Dermosifiliogr*, doi:10.1016/j.ad.2020.05.003 (2020).

48 Craver, R. *et al.* Fatal Eosinophilic Myocarditis in a Healthy 17-Year-Old Male with Severe Acute Respiratory Syndrome Coronavirus 2 (SARS-CoV-2c). *Fetal Pediatr Pathol*, 1-6, doi:10.1080/15513815.2020.1761491 (2020).

49 Dasgupta, P. & Keegan, A. D. Contribution of alternatively activated macrophages to allergic lung inflammation: a tale of mice and men. *J Innate Immun* **4**, 478-488, doi:10.1159/000336025 (2012).

50 Atyeo, C. *et al.* Distinct Early Serological Signatures Track with SARS-CoV-2 Survival. *Immunity*, doi:10.1016/j.immuni.2020.07.020 (2020).

51 Zohar, T. & Alter, G. Dissecting antibody-mediated protection against SARS-CoV-2. *Nat Rev Immunol* **20**, 392-394, doi:10.1038/s41577-020-0359-5 (2020).

52 Bournazos, S., Gupta, A. & Ravetch, J. V. The role of IgG Fc receptors in antibody-dependent enhancement. *Nat Rev Immunol*, doi:10.1038/s41577-020-00410-0 (2020).

720 53 Chang, L., Yan, Y. & Wang, L. Coronavirus Disease 2019: Coronaviruses and Blood
721 Safety. *Transfus Med Rev* **34**, 75-80, doi:10.1016/j.tmrv.2020.02.003 (2020).
722 54 Huang, C. *et al.* Clinical features of patients infected with 2019 novel coronavirus in
723 Wuhan, China. *Lancet* **395**, 497-506, doi:10.1016/S0140-6736(20)30183-5 (2020).
724 55 Chua, R. L. *et al.* COVID-19 severity correlates with airway epithelium-immune cell
725 interactions identified by single-cell analysis. *Nat Biotechnol* **38**, 970-979,
726 doi:10.1038/s41587-020-0602-4 (2020).
727 56 Liao, M. *et al.* Single-cell landscape of bronchoalveolar immune cells in patients with
728 COVID-19. *Nature medicine* **26**, 842-844, doi:10.1038/s41591-020-0901-9 (2020).
729 57 Pont, F., Tosolini, M. & Fournie, J. J. Single-Cell Signature Explorer for comprehensive
730 visualization of single cell signatures across scRNA-seq datasets. *Nucleic Acids Res* **47**,
731 e133, doi:10.1093/nar/gkz601 (2019).
732 58 Baharom, F. *et al.* Human Lung Dendritic Cells: Spatial Distribution and Phenotypic
733 Identification in Endobronchial Biopsies Using Immunohistochemistry and Flow
734 Cytometry. *Jove-J Vis Exp*, doi:ARTN e55222 10.3791/55222 (2017).
735 59 Stuart, T. *et al.* Comprehensive Integration of Single-Cell Data. *Cell* **177**, 1888-1902
736 e1821, doi:10.1016/j.cell.2019.05.031 (2019).
737 60 Liberzon, A. *et al.* The Molecular Signatures Database (MSigDB) hallmark gene set
738 collection. *Cell Syst* **1**, 417-425, doi:10.1016/j.cels.2015.12.004 (2015).
739 61 Jassal, B. *et al.* The reactome pathway knowledgebase. *Nucleic Acids Res* **48**, D498-D503,
740 doi:10.1093/nar/gkz1031 (2020).
741

Figure legends

Fig. 1. Kinetic changes of respiratory viral loads and C-reactive proteins in plasma. a. Kinetic changes of viral loads were evaluated in respiratory specimens (nasopharygeal/throat swabs for upper respiratory tract and sputa for lower respiratory tract) by quantitative RT-PCR targeting the E gene of SARS-CoV-2 and presented as Ct values. Blue circles (n = 49 and 41 for upper and lower respiratory specimens, respectively) are from eight mild patients and red circles (n = 38 and 39 for upper and lower respiratory specimens, respectively) are from five severe cases. The blue and red lines show the trend in viral load, using smoothing splines (dashed line: cut-off value). Distribution of Ct values in mild (M) and severe (S) are also presented as violin plots (right graph, black line: median). **b.** Kinetic change of C-reactive proteins (CRP) in plasma is presented. Blue circles are from nine mild patients (n = 37) and red circles are from five severe cases (n = 23). Distribution of CRP levels in mild (M) and severe (S) are also presented as violin plots (right graph, black line: median). DPS: days post symptom onset. ***: $p < 0.001$ (Two-tailed Mann–Whitney test).

Fig. 2. Kinetic changes in respiratory specimens collected from COVID-19 patients. a. Representative images of cytological analysis of sputa and BALFs by hematoxylin and eosin (H&E) staining. The patient's ID., collection day after symptom onset, and types of specimens (SPT: sputum, and BALF: bronchoalveolar lavage fluid) are presented in the upper left text box. Arrows indicate PMNs (orange, mostly neutrophils), eosinophils (red), lymphocytes (blue), and macrophages (green). Scale bar: 20 μm. **b.** Relative frequencies of the indicated leukocyte subsets among $CD45^+$ leukocytes in paired blood and BALF were analyzed by flow cytometry

764 and presented. Patients' ID. are presented at the bottom. DPS: days post symptom onset. **c and d.**
765 Kinetic changes of the indicated leukocytes in respiratory specimens are presented. All the data
766 (n = 49) from H&E staining and flow cytometry are plotted in **c.** The lines show the kinetic trend
767 of each leukocyte subset, using smoothing splines. Kinetic changes in relative frequencies of the
768 indicated leukocyte subsets in mild (blue, n = 20) and severe (red, n = 29) groups are presented
769 in **d**. DPS: days post symptom onset.
770
771 **Fig. 3. Kinetic profiling of inflammatory mediators derived from inflammatory leukocytes**
772 **in respiratory specimens.** Kinetic changes of inflammatory mediators or biomarkers derived
773 from neutrophils (**a**), eosinophils (**b**), mast cells (**c**), macrophages (**d**), and cytotoxic T cells/NK
774 cells (**e**) in respiratory specimens are presented. Concentrations of inflammatory markers in mild
775 (M) and severe (S) cases are also compared and presented as violin plots (right graph, black line:
776 median). The lines show the kinetic trend, using smoothing splines. LCN: lipocalin-2 (n = 18 for
777 mild and 23 for severe cases), CALP: calprotectin (n = 11 for mild and 19 for severe cases),
778 EDN: eosinophil-derived neurotoxin (n = 18 for mild and 23 for severe cases), ECP: eosinophilic
779 cationic protein (n = 11 for mild and 19 for severe cases), MCT: mast cell tryptase (n = 18 for
780 mild and 23 for severe cases). sCD163 and granzyme A (n = 18 for mild and 23 for severe cases).
781 DPS: days post symptom onset. *: $p < 0.05$ (two-tailed Mann–Whitney test).
782
783 **Fig. 4. Correlation of respiratory levels of cytokines, chemokines, and inflammatory**
784 **mediators in COVID-19 patients. a.** Correlation matrix of 28 inflammatory proteins detected in
785 respiratory samples from COVID-19 patients (see raw data in Supplementary Table S3). The
786 areas of the circles show the value of corresponding correlation coefficients as calculated by the

Spearman method. Positive correlations are displayed in blue and negative correlations in red. The size of the circle and intensity of color are proportional to correlation coefficients (0 to 1 for positive coefficient and 0 to -1 for negative coefficient). The legend to the right of the matrix shows the Spearman correlation coefficients for the corresponding colors. The correlation coefficients of proteins were clustered based on hierarchical clustering. Boxes indicate groups of cytokines with higher correlations. * : $p < 0.05$, ** : $p < 0.01$, *** : $p < 0.001$. **b.** Kinetic changes of IL-6 and TGF-β, cytokines showing significant difference between mild (blue, M, $n = 11$) and severe (red, S, $n = 20$) groups. The lines show the kinetic trend, using smoothing splines. Concentrations of the cytokines in mild and severe were also compared and presented as violin plots (right graph, black line: median). DPS: days post symptom onset.

Fig. 5. Kinetic changes of SARS-CoV-2 N-specific antibodies and C3a in respiratory specimens. Kinetic changes in specific antibody responses against viral N protein (**a**) and C3a (**b**) in respiratory samples are presented. Specific isotypes of the antigen-specific antibodies are denoted. Blue: mild ($n = 13$ for antibodies and 20 for C3a), red: severe ($n = 28$ for antibodies and 20 for C3a). The lines show the kinetic trend, using smoothing splines. The levels in mild and severe cases were also compared and presented as violin plots (right side, black line: median). *: $p < 0.05$ (Two-tailed Mann–Whitney test). DPS: days post symptom onset. **c.** Correlation of C3a levels with N-specific IgM (left) and IgG (right) were assessed by linear regression (dashed line) and Spearman's rank test. p values are indicated within the graphs. $n = 27$.

Fig. 6. Kinetic changes of SARS-CoV-2 N-specific antibodies and C3a in plasma. Kinetic changes in specific antibody responses against viral N protein (**a**), C3a and C5a (**b**) in plasma

samples are presented. Specific isotypes of the antigen-specific antibodies are denoted. Blue: mild (n = 30), red: severe (n = 19). The lines show the kinetic trend, using smoothing splines. The levels in mild and severe cases were also compared and presented as violin plots (right side, black line: median). DPS: days post symptom onset. * : $p < 0.05$, ** : $p < 0.01$, *** : $p < 0.001$ (Two-tailed Mann–Whitney test). **c.** Correlation of C5a levels with N-specific IgG1 (left) and IgG3 (right) were assessed by linear regression (dashed line) and Spearman's rank test. p values are indicated within the graphs. n = 61.

Fig. 7. Kinetic changes of viral loads, inflammatory indicators, antibody responses, and pulmonary histopathology in a fatal COVID-19 case. a. Kinetic changes of viral loads were evaluated in respiratory specimens in upper respiratory (U.R.) and lower respiratory (L.R.) tract (black dashed line: cut-off value). Kinetic change of CRP in plasma is also presented (red dashed line: upper limit of normal range, 10 mg/dL). **b.** Kinetic changes of lactate dehydrogenase (LDH, red) and creatine phosphokinase (CPK, blue) in plasma. Blue and red dashed lines indicates upper limit of normal ranges for CPK (200 U/L) and LDH (350 U/L), respectively. Microscopic findings in H&E-stained lung tissues from a fatal case, P15, obtained at D36 (**c**) and D48 (**d**) after symptom onset. At a scan view, subpleural lung parenchyma with fibrosis and fibrin deposits are observed (upper left, 12.5x magnification). Higher power views of each representative area (rectangles) are displayed. **c.** Fibrinous exudate, hemorrhage and congestion in subpleural lung parenchyma are observed (upper right, 200x). A few alveolar macrophages and hemorrhage in intra-alveolar spaces (black arrow) and some lymphoplasmacytic infiltration and smooth muscle proliferation in dense fibrotic interstitium are observed (lower left, 200x). A few neutrophilic infiltration (red arrows) and congested blood vessels reminiscent of granulation

tissue are noted (lower right, 400x). **d.** Marked intra-alveolar hemorrhage and congestion in blood vessels are observed along with interstitial thickening and fibrosis (upper right, 200x). In non-hemorrhagic areas, interstitial thickening and fibrosis, alveolar bronchiolization (black arrows), intra-alveolar seromucinous fluid accumulation and variable-sized alveolar macrophages (asterisks) are observed. Infiltration of a few lymphoid cells and plasma cells in interstitium is noted (blue arrow) (lower left, 200x). Alveolar bronchiolization (bronchiolar metaplasia of alveoli) (black arrows), detachment of alveolar epithelial cells (green arrows) and interstitial thickening and fibrosis (asterisks) are observed (lower right, 200x). **e.** Kinetic changes in specific antibody responses against viral N protein and C5a in respiratory samples (left) and plasma (right). **f.** Localization of SARS-CoV-2 N antigens in lung tissues. Representative images of triple immunofluorescence-stained sections of lung tissues obtained from the fatal case at D36 (upper panels) and D48 (lower panels). Immunofluorescence for endothelial marker (CD31, green, left panels) or epithelial marker (CK: pan-cytokeratin, green, right panels), together with SARS-CoV-2 N antigens (red), are indicated. Nuclear DNA was counterstained with 4,6-diamidino-2-phenylindole (blue). Differential interference contrast (DIC) images show lung parenchyma. Blood vessels are indicated by white asterisks. Scale bar, 100 μm.

Fig. 8. Pathologic association of complement activation and immune complexes deposition as identified by immunohistochemistry and immunofluorescence analysis of pulmonary autopsy samples from a fatal COVID-19 case. a. Immunohistochemical detection of C5b-9 membrane attack complexes in pulmonary parenchyma using lung tissues from a fatal case obtained at D36 (left panels) and D48 (right panels). C5b-9 staining was observed in media layer of vascular walls (asterisks), airway epithelial cells (purple arrows), and inflammatory cells such

as macrophages (green arrows) and lymphoplasma cells (red arrows). Scale bar: 100 μm. **b.** Depositions of IgG immune complexes in airways and blood vessels were identified by immunofluorescence analysis. Representative immunofluorescence images of lung tissues obtained from the fatal case at D36 (upper panels) and D48 (lower panels) are presented. Immunofluorescence of epithelial marker (CK: pan-cytokeratin, green, right panels), SARS-CoV-2 N antigens (red), and IgG (white) are indicated. White arrows indicate depositions of IgG immune complexes in the luminal spaces, hyaline membranes, and fibrin deposits. Nuclear DNA was counterstained with 4,6-diamidino-2-phenylindole (blue). Differential interference contrast (DIC) images show lung parenchyma. Blood vessels are indicated by white asterisks. Scale bar, 100 μm.

Fig. 9. Enhanced gene set signatures for FcγR signaling and complement activation in myeloid cells of respiratory samples from severe COVID-19 cases. a. UMAP presentation of major cell types and associated clusters in respiratory leukocytes from COVID-19 patients. Data sets were retrieved from two previous studies.[55,56] Ep.: epithelial cells, B: B cells, T.NK: T and NK cells, Mo.MF.DC: monocytes, macrophages, and dendritic cells, Neutro.: neutrophils. **b.** Hallmark gene set scores for inflammatory response, computed for the indicated leukocyte subsets (all patients' samples combined), were compared with those of healthy controls (HC). *p* values for differences between HC and COVID-19 patients as assessed by two-tailed Mann–Whitney U test are presented. **c.** Computed hallmark gene set activity scores of FcγR signaling and complement activation, for the indicated myeloid subsets. *P* values for differences among HC and COVID-19 patients with mild (M) or severe (S) symptoms, as assessed by two-tailed

878 Mann–Whitney U test, are presented.

879

880

881

882

883

884

885

886

887

888

889

890

891

892

893

894

895

896

897

898

899

900

Supplementary Information

Table S1. Baseline characteristics of COVID-19 patients included in this study.

Table S2. Summary of cytological analysis of sputa and BALFs by hematoxylin and eosin (H&E) staining.

Table S3. Raw data of 28 cytokines, chemokines, and inflammatory mediators measured in respiratory specimens collected from COVID-19 patients.

Fig. S1. Clinical courses of group 1 patients with COVID-19 enrolled in the present study.

Fig. S2. Gating strategy for the characterization of leukocytes in blood and BALFs.

Fig. S3. Relative frequencies of myeloid cell subtypes in blood and BALF specimens from patients with severe COVID-19. The frequencies are percentile among $CD45^+$ leukocytes.

Fig. S4. Relative frequencies of lymphoid cell subtypes in blood and BALF specimens from patients with severe COVID-19. The frequencies are percentile among lymphocytes.

Fig. S5. Relative frequencies of T and NKT cell subtypes in blood and BALF specimens from patients with severe COVID-19. The frequencies are percentile among lymphocytes.

Fig. S6. Kinetic changes of 28 cytokines, chemokines, and inflammatory mediators measured in respiratory specimens collected from COVID-19 patients. Raw data for each graph are presented in Supplementary Table S3. The purple lines show the kinetic trend of each inflammatory marker, using smoothing splines. Blue dots: mild cases, red dots: severe cases. n.d.: not detected.

Fig. S7. Kinetic changes of specific antibodies against viral N protein in plasma from COVID-19 patients. Specific isotypes of the antigen-specific antibodies are indicated. Blue are from eight

mild patients and red are from five severe cases.

Fig. S8. Kinetics of complete blood counts in blood collected from COVID-19 patients. Normal range of each leukocyte count is indicated as gray background.

Fig. S9. Depositions of IgG immune complexes in lung tissue were identified by immunofluorescence analysis. Representative immunofluorescence images of lung tissue obtained from the fatal case at D48 are presented. Immunofluorescence of SARS-CoV-2 N antigens (red) and IgG (white) are indicated. Blue: nuclei, DIC: Differential interference contrast, scale bar: 100 μm.

Figures

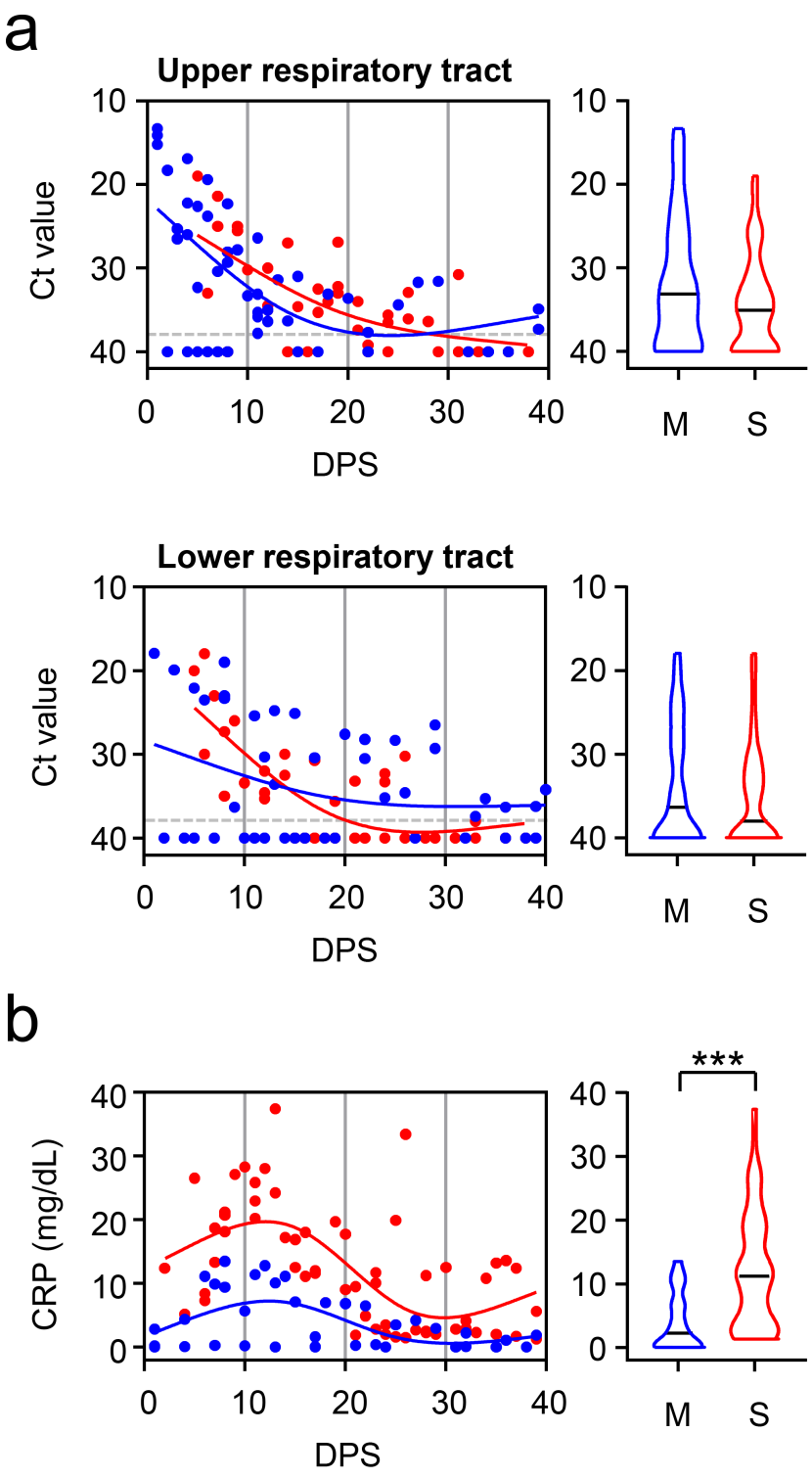

Figure 1

Kinetic changes of respiratory viral loads and C-reactive proteins in plasma. a. Kinetic changes of viral loads were evaluated in respiratory specimens (nasopharygeal/throat swabs for upper respiratory tract and sputa for lower respiratory tract) by quantitative RT-PCR targeting the E gene of SARS-CoV-2 and

presented as Ct values. Blue circles (n = 49 and 41 for upper and lower respiratory specimens, respectively) are from eight mild patients and red circles (n = 38 and 39 for upper and lower respiratory specimens, respectively) are from five severe cases. The blue and red lines show the trend in viral load, using smoothing splines (dashed line: cut-off value). Distribution of Ct values in mild (M) and severe (S) are also presented as violin plots (right graph, black line: median). b. Kinetic change of C-reactive proteins (CRP) in plasma is presented. Blue circles are from nine mild patients (n = 37) and red circles are from five severe cases (n = 23). Distribution of CRP levels in mild (M) and severe (S) are also presented as violin plots (right graph, black line: median). DPS: days post symptom onset. ***: $p < 0.001$ (Two-tailed Mann–Whitney test).

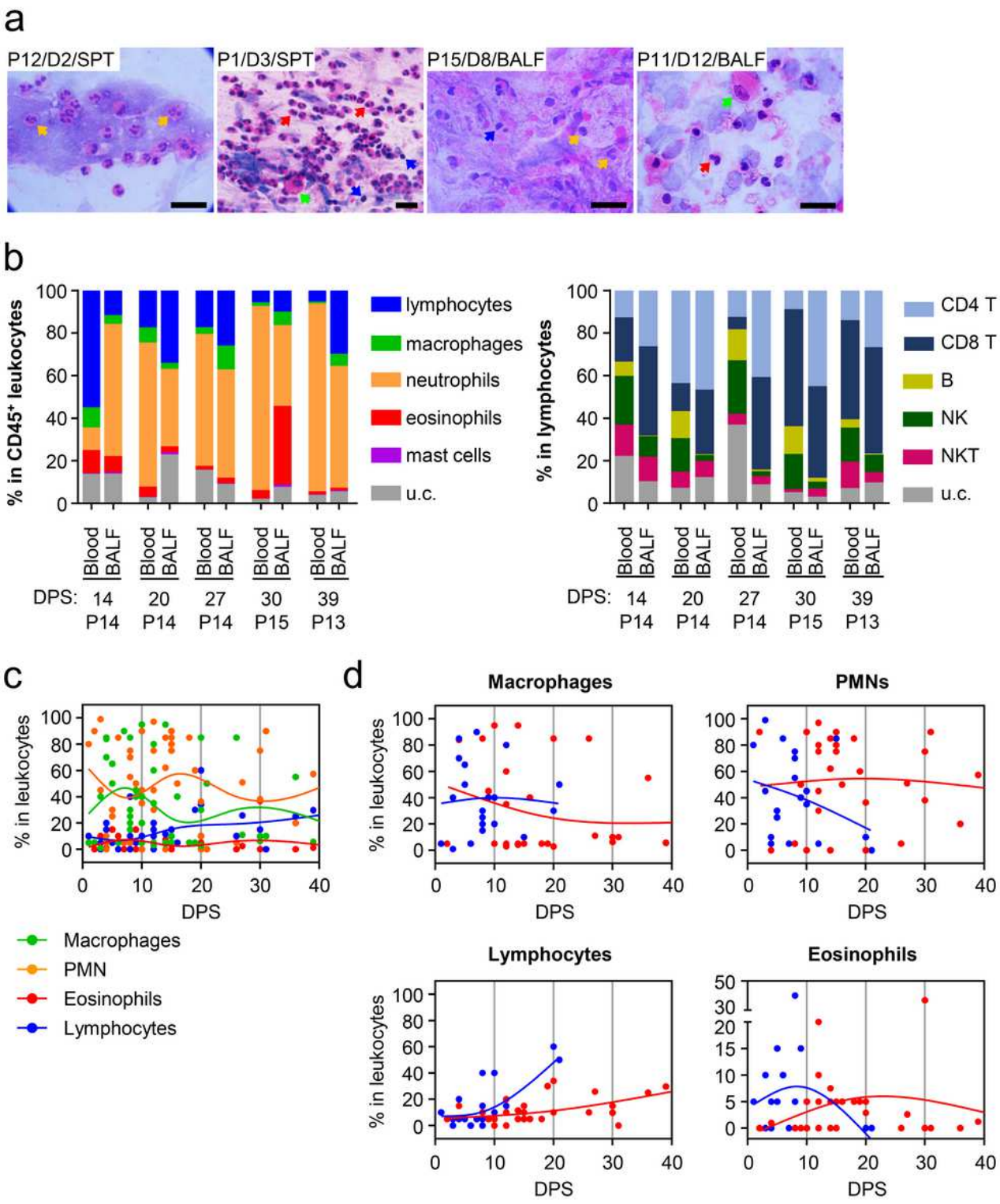

Figure 2

Kinetic changes in respiratory specimens collected from COVID-19 patients. a. Representative images of cytological analysis of sputa and BALFs by hematoxylin and eosin (H&E) staining. The patient's ID., collection day after symptom onset, and types of specimens (SPT: sputum, and BALF: bronchoalveolar lavage fluid) are presented in the upper left text box. Arrows indicate PMNs (orange, mostly neutrophils), eosinophils (red), lymphocytes (blue), and macrophages (green). Scale bar: 20 μm. b. Relative

frequencies of the indicated leukocyte subsets among CD45+ leukocytes in paired blood and BALF were analyzed by flow cytometry and presented. Patients' ID. are presented at the bottom. DPS: days post symptom onset. c and d. Kinetic changes of the indicated leukocytes in respiratory specimens are presented. All the data (n = 49) from H&E staining and flow cytometry are plotted in c. The lines show the kinetic trend of each leukocyte subset, using smoothing splines. Kinetic changes in relative frequencies of the indicated leukocyte subsets in mild (blue, n = 20) and severe (red, n = 29) groups are presented in d. DPS: days post symptom onset.

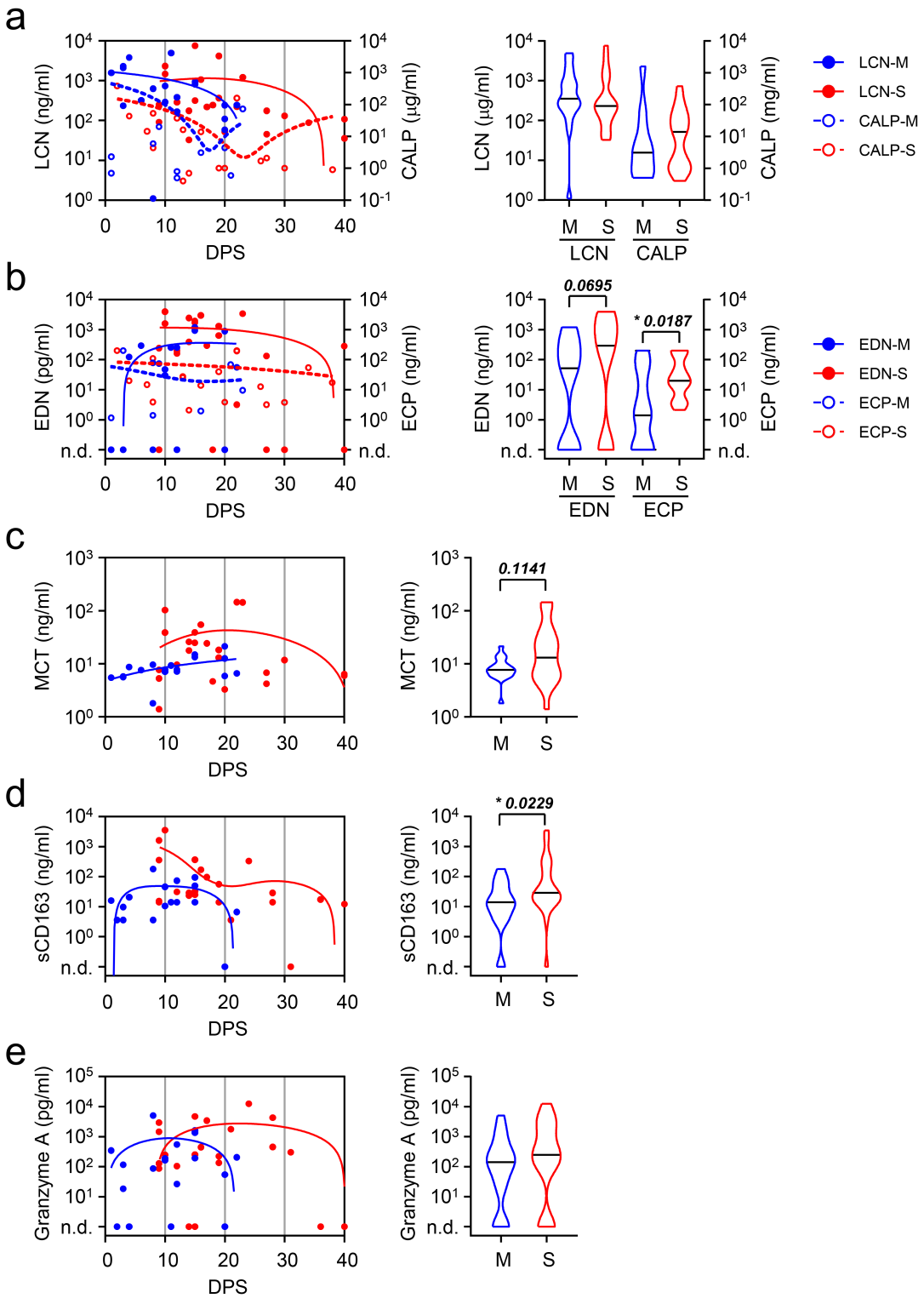

Figure 3

Kinetic profiling of inflammatory mediators derived from inflammatory leukocytes in respiratory specimens. Kinetic changes of inflammatory mediators or biomarkers derived from neutrophils (a), eosinophils (b), mast cells (c), macrophages (d), and cytotoxic T cells/NK cells (e) in respiratory specimens are presented. Concentrations of inflammatory markers in mild (M) and severe (S) cases are also compared and presented as violin plots (right graph, black line: median). The lines show the kinetic trend, using smoothing splines. LCN: lipocalin-2 (n = 18 for mild and 23 for severe cases), CALP: calprotectin (n = 11 for mild and 19 for severe cases), EDN: eosinophil-derived neurotoxin (n = 18 for mild and 23 for severe cases), ECP: eosinophilic cationic protein (n = 11 for mild and 19 for severe cases), MCT: mast cell tryptase (n = 18 for mild and 23 for severe cases). sCD163 and granzyme A (n = 18 for mild and 23 for severe cases). DPS: days post symptom onset. *: $p < 0.05$ (two-tailed Mann–Whitney test).

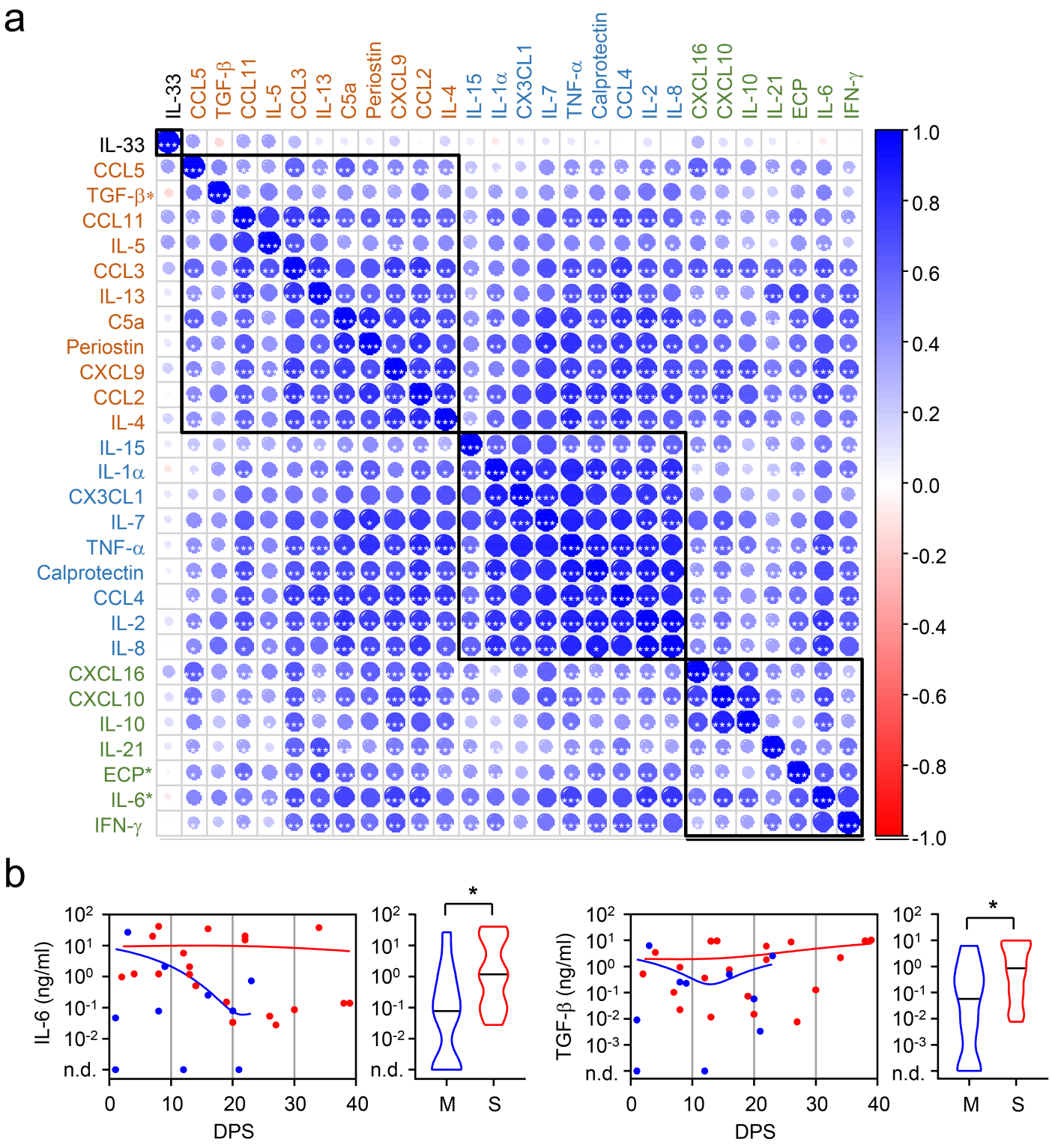

Figure 4

Correlation of respiratory levels of cytokines, chemokines, and inflammatory mediators in COVID-19 patients. a. Correlation matrix of 28 inflammatory proteins detected in respiratory samples from COVID-19 patients (see raw data in Supplementary Table S3). The areas of the circles show the value of corresponding correlation coefficients as calculated by the Spearman method. Positive correlations are displayed in blue and negative correlations in red. The size of the circle and intensity of color are

proportional to correlation coefficients (0 to 1 for positive coefficient and 0 to -1 for negative coefficient). The legend to the right of the matrix shows the Spearman correlation coefficients for the corresponding colors. The correlation coefficients of proteins were clustered based on hierarchical clustering. Boxes indicate groups of cytokines with higher correlations. * : $p < 0.05$, ** : $p < 0.01$, *** : $p < 0.001$. b. Kinetic changes of IL-6 and TGF-β cytokines showing significant difference between mild (blue, M, n = 11) and severe (red, S, n = 20) groups. The lines show the kinetic trend, using smoothing splines. Concentrations of the cytokines in mild and severe were also compared and presented as violin plots (right graph, black line: median). DPS: days post symptom onset.

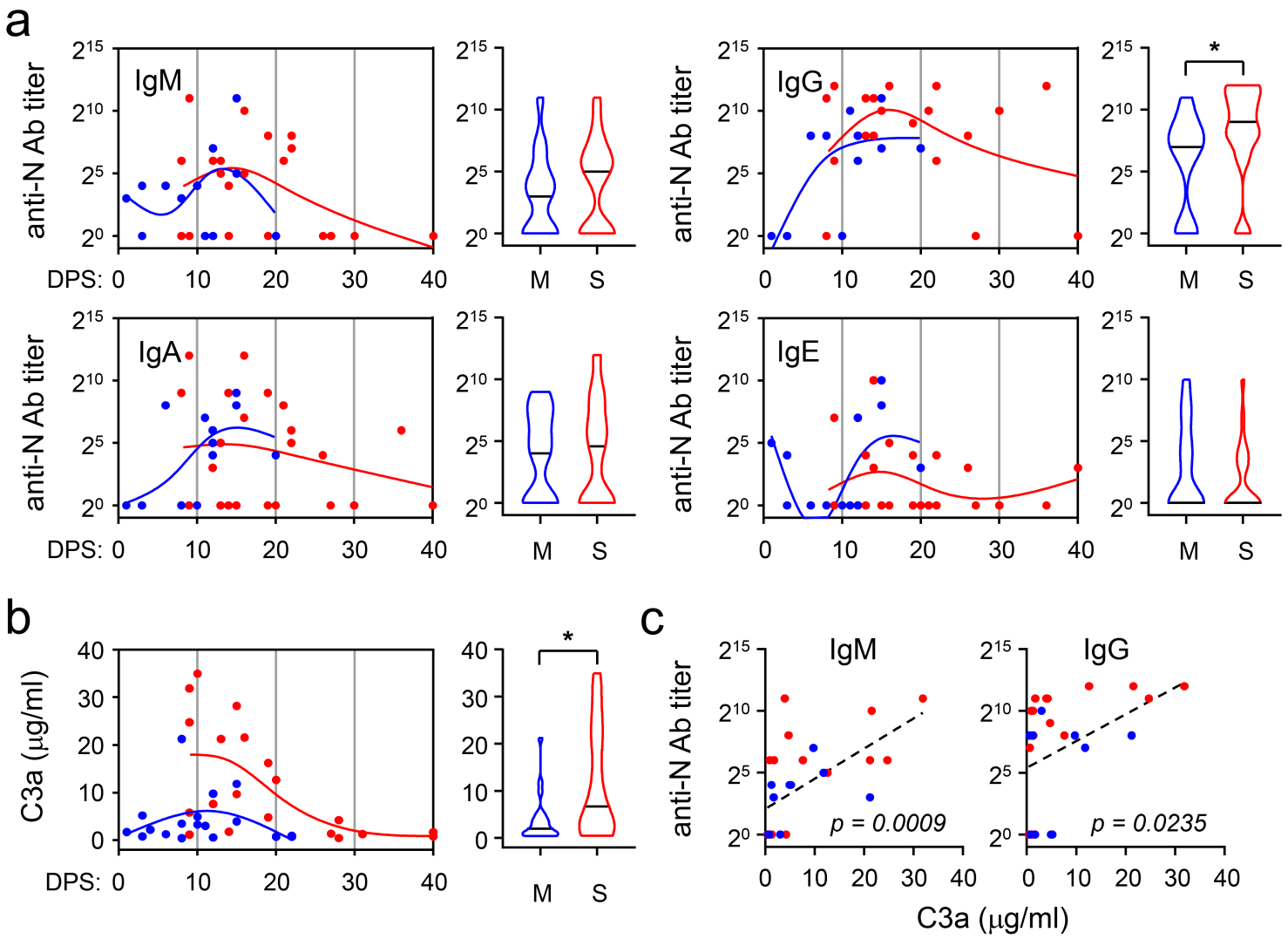

Figure 5

Kinetic changes of SARS-CoV-2 N-specific antibodies and C3a in respiratory specimens. Kinetic changes in specific antibody responses against viral N protein (a) and C3a (b) in respiratory samples are presented. Specific isotypes of the antigen-specific antibodies are denoted. Blue: mild (n = 13 for antibodies and 20 for C3a), red: severe (n = 28 for antibodies and 20 for C3a). The lines show the kinetic trend, using smoothing splines. The levels in mild and severe cases were also compared and presented as violin plots (right side, black line: median). *: $p < 0.05$ (Two-tailed Mann–Whitney test). DPS: days post

symptom onset. c. Correlation of C3a levels with N-specific IgM (left) and IgG (right) were assessed by linear regression (dashed line) and Spearman's rank test. p values are indicated within the graphs. n = 27.

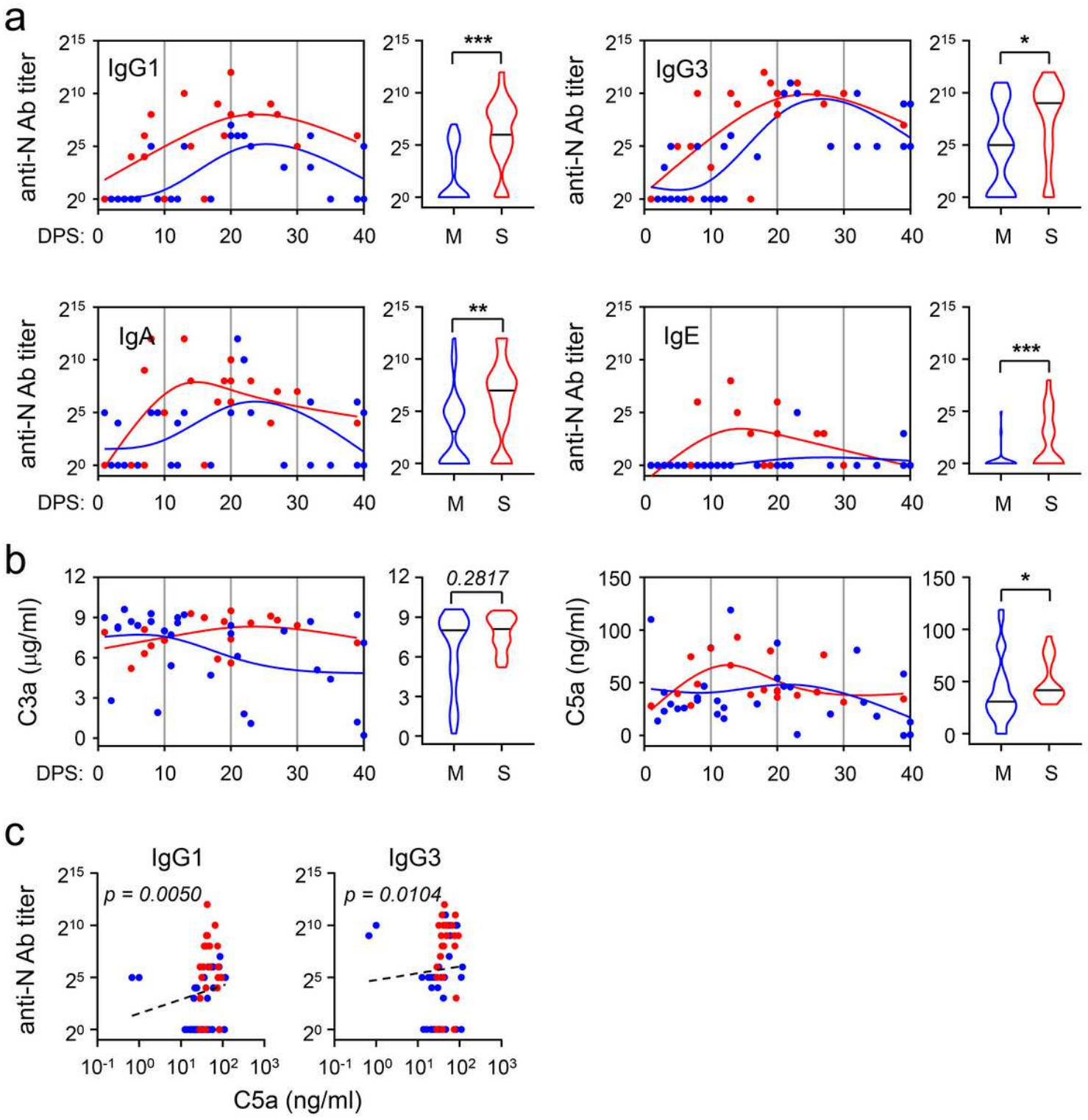

Figure 6

Kinetic changes of SARS-CoV-2 N-specific antibodies and C3a in plasma. Kinetic changes in specific antibody responses against viral N protein (a), C3a and C5a (b) in plasma samples are presented. Specific isotypes of the antigen-specific antibodies are denoted. Blue: mild (n = 30), red: severe (n = 19).

The lines show the kinetic trend, using smoothing splines. The levels in mild and severe cases were also compared and presented as violin plots (right side, black line: median). DPS: days post symptom onset. * : $p < 0.05$, ** : $p < 0.01$, *** : $p < 0.001$ (Two-tailed Mann–Whitney test). c. Correlation of C5a levels with N-specific IgG1 (left) and IgG3 (right) were assessed by linear regression (dashed line) and Spearman's rank test. p values are indicated within the graphs. n = 61.

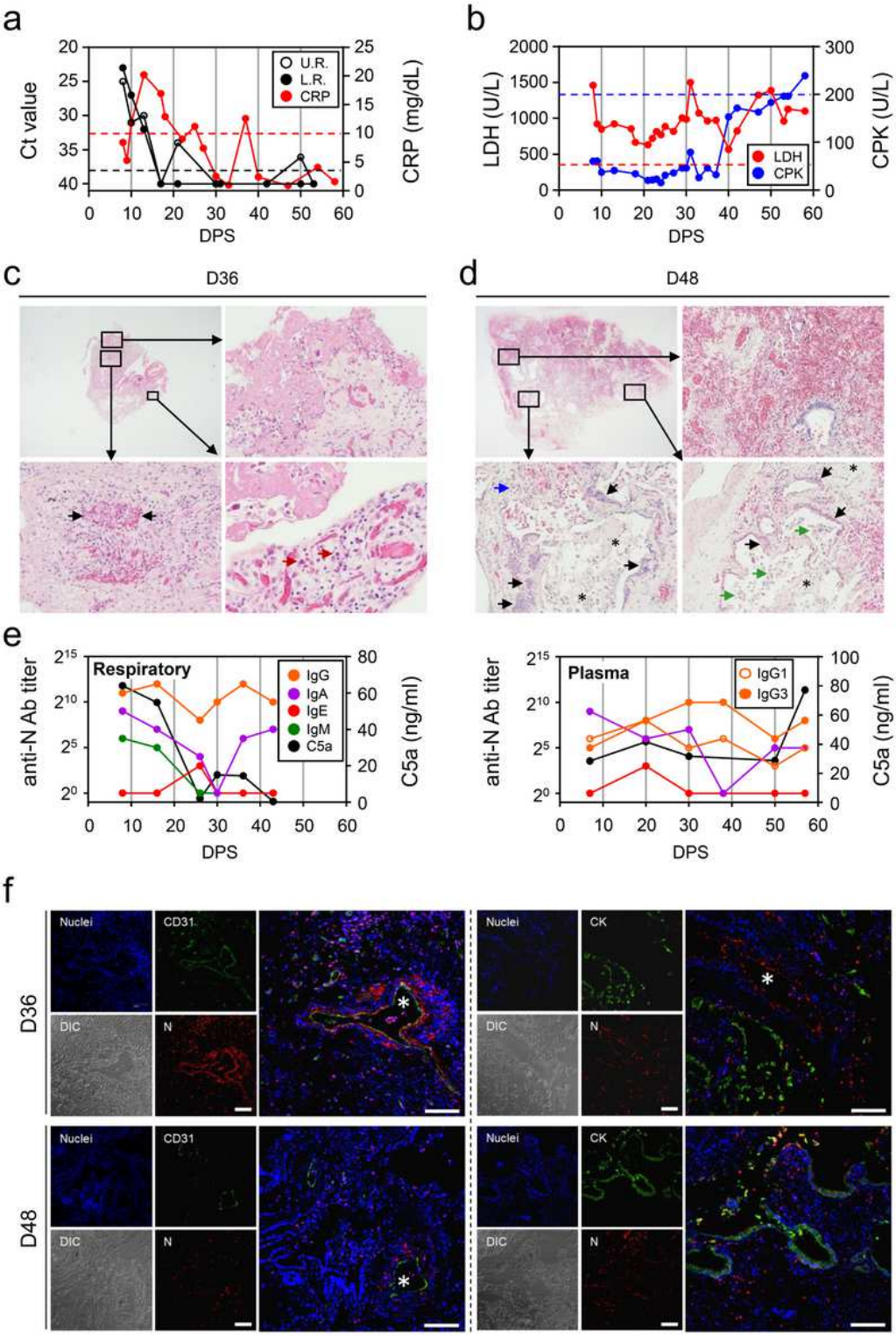

Figure 7

Kinetic changes of viral loads, inflammatory indicators, antibody responses, and pulmonary histopathology in a fatal COVID-19 case. a. Kinetic changes of viral loads were evaluated in respiratory specimens in upper respiratory (U.R.) and lower respiratory (L.R.) tract (black dashed line: cut-off value). Kinetic change of CRP in plasma is also presented (red dashed line: upper limit of normal range, 10 mg/dL). b. Kinetic changes of lactate dehydrogenase (LDH, red) and creatine phosphokinase (CPK, blue) in plasma. Blue and red dashed lines indicates upper limit of normal ranges for CPK (200 U/L) and LDH (350 U/L), respectively. Microscopic findings in H&E-stained lung tissues from a fatal case, P15, obtained at D36 (c) and D48 (d) after symptom onset. At a scan view, subpleural lung parenchyma with fibrosis and fibrin deposits are observed (upper left, 12.5x magnification). Higher power views of each representative area (rectangles) are displayed. c. Fibrinous exudate, hemorrhage and congestion in subpleural lung parenchyma are observed (upper right, 200x). A few alveolar macrophages and hemorrhage in intra-alveolar spaces (black arrow) and some lymphoplasmacytic infiltration and smooth muscle proliferation in dense fibrotic interstitium are observed (lower left, 200x). A few neutrophilic infiltration (red arrows) and congested blood vessels reminiscent of granulation tissue are noted (lower right, 400x). d. Marked intra-alveolar hemorrhage and congestion in blood vessels are observed along with interstitial thickening and fibrosis (upper right, 200x). In non-hemorrhagic areas, interstitial thickening and fibrosis, alveolar bronchiolization (black arrows), intra-alveolar seromucinous fluid accumulation and variable-sized alveolar macrophages (asterisks) are observed. Infiltration of a few lymphoid cells and plasma cells in interstitium is noted (blue arrow) (lower left, 200x). Alveolar bronchiolization (bronchiolar metaplasia of alveoli) (black arrows), detachment of alveolar epithelial cells (green arrows) and interstitial thickening and fibrosis (asterisks) are observed (lower right, 200x). e. Kinetic changes in specific antibody responses against viral N protein and C5a in respiratory samples (left) and plasma (right). f. Localization of SARS-CoV-2 N antigens in lung tissues. Representative images of triple immunofluorescence-stained sections of lung tissues obtained from the fatal case at D36 (upper panels) and D48 (lower panels). Immunofluorescence for endothelial marker (CD31, green, left panels) or epithelial marker (CK: pan-cytokeratin, green, right panels), together with SARS-CoV-2 N antigens (red), are indicated. Nuclear DNA was counterstained with 4,6-diamidino-2-phenylindole (blue). Differential interference contrast (DIC) images show lung parenchyma. Blood vessels are indicated by white asterisks. Scale bar, 100 μm.

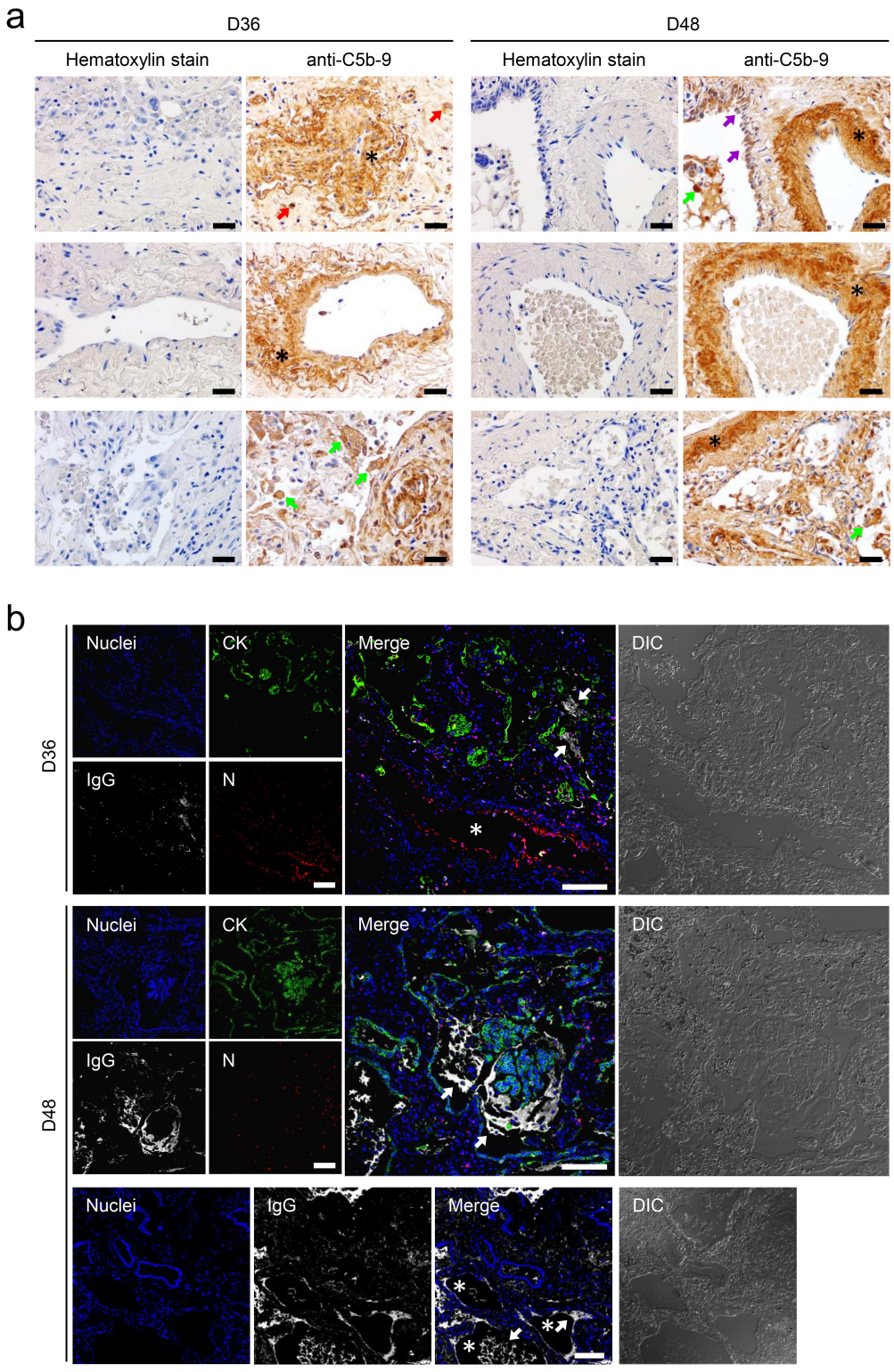

Figure 8

Pathologic association of complement activation and immune complexes deposition as identified by immunohistochemistry and immunofluorescence analysis of pulmonary autopsy samples from a fatal COVID-19 case. a. Immunohistochemical detection of C5b-9 membrane attack complexes in pulmonary parenchyma using lung tissues from a fatal case obtained at D36 (left panels) and D48 (right panels). C5b-9 staining was observed in media layer of vascular walls (asterisks), airway epithelial cells (purple

arrows), and inflammatory cells such as macrophages (green arrows) and lymphoplasma cells (red arrows). Scale bar: 100 μm. b. Depositions of IgG immune complexes in airways and blood vessels were identified by immunofluorescence analysis. Representative immunofluorescence images of lung tissues obtained from the fatal case at D36 (upper panels) and D48 (lower panels) are presented. Immunofluorescence of epithelial marker (CK: pan-cytokeratin, green, right panels), SARS-CoV-2 N antigens (red), and IgG (white) are indicated. White arrows indicate depositions of IgG immune complexes in the luminal spaces, hyaline membranes, and fibrin deposits. Nuclear DNA was counterstained with 4,6-diamidino-2-phenylindole (blue). Differential interference contrast (DIC) images show lung parenchyma. Blood vessels are indicated by white asterisks. Scale bar, 100 μm.

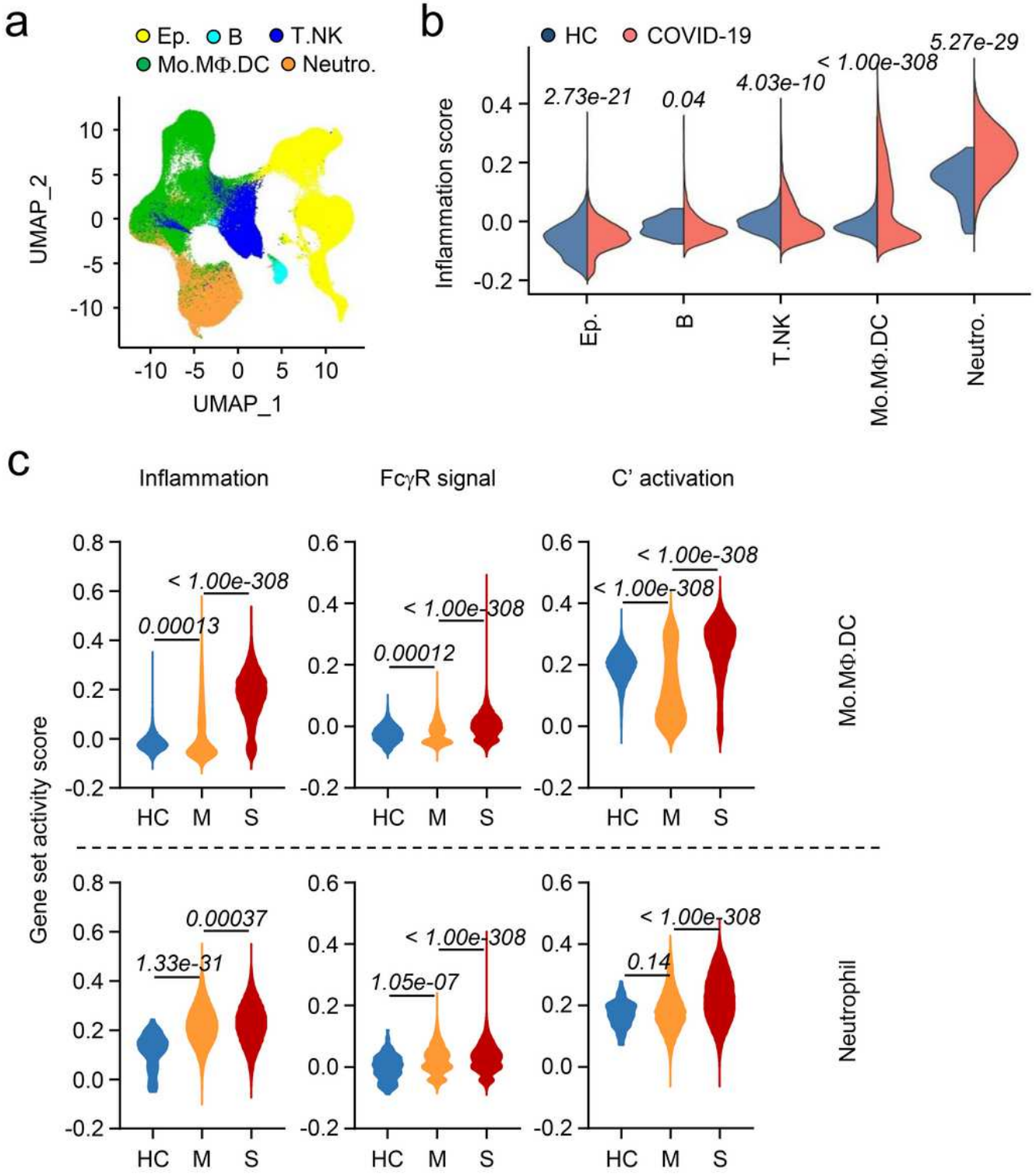

Figure 9

Enhanced gene set signatures for FcγR signaling and complement activation in myeloid cells of respiratory samples from severe COVID-19 cases. a. UMAP presentation of major cell types and associated clusters in respiratory leukocytes from COVID-19 patients. Data sets were retrieved from two previous studies.55,56 Ep.: epithelial cells, B: B cells, T.NK: T and NK cells, Mo.MF.DC: monocytes, macrophages, and dendritic cells, Neutro.: neutrophils. b. Hallmark gene set scores for inflammatory

response, computed for the indicated leukocyte subsets (all patients' samples combined), were compared with those of healthy controls (HC). p values for differences between HC and COVID-19 patients as assessed by two-tailed Mann–Whitney U test are presented. c. Computed hallmark gene set activity scores of FcγR signaling and complement activation, for the indicated myeloid subsets. P values for differences among HC and COVID-19 patients with mild (M) or severe (S) symptoms, as assessed by two-tailed Mann–Whitney U test, are presented.

Supplementary Files

This is a list of supplementary files associated with this preprint. Click to download.

- SupplementaryFigures.pdf
- SupplementaryTableS13.xls